1997-06

Evaluating the role of NAT, NAD, and liquid H2SO4/H2O/HNO3 solutions in Antarctic polar stratospheric cloud aerosol: Observations and implications

JOURNAL OF GEOPHYSICAL RESEARCH, VOL. 102, NO. D11, PAGES 13,255–13,282, JUNE 20, 1997

Evaluating the role of NAT, NAD, and liquid $H_2SO_4/H_2O/HNO_3$ solutions in Antarctic polar stratospheric cloud aerosol: Observations and implications

L. A. Del Negro,[1,2,3] D. W. Fahey,[1] S. G. Donnelly,[1,2] R. S. Gao,[1,2] E. R. Keim,[1] R. C. Wamsley,[1,2] E. L. Woodbridge,[4] J. E. Dye,[5] D. Baumgardner,[5] B. W. Gandrud,[5] J. C. Wilson,[6] H. H. Jonsson,[6] M. Loewenstein,[7] J. R. Podolske,[7] C. R. Webster,[8] R. D. May,[8] D. R. Worsnop,[9] A. Tabazadeh,[7] M. A. Tolbert,[2,3] K. K. Kelly,[1] and K R. Chan[7]

Abstract. Airborne measurements of total reactive nitrogen (NO_y) and polar stratospheric cloud (PSC) aerosol particles were made in the Antarctic (68°S) as part of the NASA Airborne Southern Hemisphere Ozone Experiment/Measurements for Assessing the Effects of Stratospheric Aircraft (ASHOE/MAESA) campaign in late July 1994. As found in both polar regions during previous studies, substantial PSC aerosol volume containing NO_y was observed at temperatures above the frost point, confirming the presence of particles other than water ice. The composition of the aerosol particles is evaluated using equilibrium expressions for nitric acid trihydrate (NAT), nitric acid dihydrate (NAD), and the supercooled ternary solution (STS) composed of nitric acid (HNO_3), sulfuric acid (H_2SO_4), and water (H_2O). The equilibrium abundance of condensed HNO_3 is calculated for each phase and compared to estimates made using observations of aerosol volume and NO_y. The best agreement is found for STS composition, using criteria related to the onset and abundance of aerosol volume along the flight track. Throughout the PSC region, a comparison of the number of particles between 0.4 and 4.0 μm diameter with the number of available nuclei indicates that a significant fraction of the background aerosol number participates in PSC growth. Modeled STS size distributions at temperatures below 191 K compare favorably with measured size distributions of PSC aerosol. Calculations of the heterogeneous loss of chlorine nitrate ($ClONO_2$) show that the reactivity of the observed PSC surface area is 30 to 300% greater with STS than with NAT composition for temperatures less than 195 K. The total volume of STS PSCs is shown to be more sensitive than NAT to increases in H_2O, HNO_3, and H_2SO_4 from supersonic aircraft fleet emissions. Using the current observations and perturbations predicted by the current aircraft assessments, an increase of 50 to 260% in STS aerosol volume is expected at the lowest observed temperatures (190 to 192 K), along with an extension of significant PSC activity to regions ~0.7 K higher in temperature. These results improve our understanding of PSC aerosol formation in polar regions while strengthening the requirement to include STS aerosols in studies of polar ozone loss and the effects of aircraft emissions.

Introduction

Heterogeneous reactions on polar stratospheric clouds (PSCs) play an important role in ozone destruction in both the Arctic and the Antarctic by directly activating chlorine and by sequestering nitrogen oxide (NO_x) species that moderate ozone destruction [*Toon et al.*, 1986; *Solomon*, 1988, 1990]. While the nature of these heterogeneous reactions are well established, their rates depend on the composition and phase of the PSC aerosol [*Ravishankara and Hanson*, 1996]. PSCs fall into two general categories, designated Type I and Type II. The composition of Type II PSCs is known to be water ice [*Poole and McCormick*, 1988], but that of Type I PSCs, which form at higher temperatures than water ice, remains less certain. The formation of Type I PSCs at temperatures higher than the ice frost point has been explained in theoretical work [*Crutzen and Arnold*, 1986; *Toon et al.*, 1986; *McElroy et al.*, 1986] as that of nitric acid hydrates. The laboratory work of *Hanson and Mauersberger* [1988] showed that nitric acid trihydrate ($HNO_3 \cdot 3H_2O$, NAT) could form at temperatures close to 195 K, and in situ measurements have established that Type I PSCs contain mixtures of reactive nitrogen (NO_y) and H_2O [*Fahey et al.*, 1989a; *Pueschel et al.*, 1989]. On the basis of this evidence, the composition of Type I PSCs has been widely considered to be NAT in previous analyses of field observa-

[1]Aeronomy Laboratory, National Oceanic and Atmospheric Administration, Boulder, Colorado.
[2]Cooperative Institute for Research in Environmental Science, University of Colorado, Boulder.
[3]Department of Chemistry and Biochemistry, University of Colorado, Boulder.
[4]Scripps Institution of Oceanography, University of California at San Diego, La Jolla, California.
[5]National Center for Atmospheric Research, Boulder, Colorado.
[6]Department of Engineering, University of Denver, Denver, Colorado.
[7]NASA Ames Research Center, Moffett Field, California.
[8]Jet Propulsion Laboratory, Pasadena, California.
[9]Aerodyne Research, Inc., Billerica, Massachusetts.

Paper number 97JD00764.
0148-0227/97/97JD-00764$09.00

tions within PSCs [*Fahey et al.*, 1989a; *Kawa et al.*, 1992; *Dye et al.*, 1992].

During the Airborne Antarctic Ozone Experiment (AAOE) in 1987, measurements of NO_y, total H_2O, and aerosol and meteorological parameters were obtained in a PSC [*Fahey et al.*, 1989a]. Significant increases in aerosol volume indicated the presence of a PSC, and evidence of condensed NO_y species was found for temperatures just below those corresponding to NAT saturation conditions [*Hanson and Mauersberger*, 1988]. Different results were found during the 1988-1989 Airborne Arctic Stratospheric Expedition (AASE). In the Arctic data, conditions were supersaturated with respect to NAT by greater than a factor of 10 when a significant increase in aerosol volume was observed. To explain this supersaturation, a nucleation barrier to NAT crystallization was proposed, as well as the possibility that frozen sulfuric acid (H_2SO_4) aerosols were required as condensation nuclei [*Kawa et al.*, 1992; *Dye et al.*, 1992].

Laboratory studies have confirmed that supersaturation conditions occur either prior to or during NAT growth on surfaces [*Hanson*, 1992]. Studies by *Iraci et al.* [1995] on thin films and by *Molina et al.* [1993] in seeding experiments have demonstrated that frozen sulfuric acid tetrahydrate (SAT) surfaces do not nucleate NAT at stratospheric temperatures and pressures. As a result, additional mechanisms for PSC formation, including other condensed phases, have been proposed to account for the apparent discrepancy between the Antarctic and the Arctic data sets. *Worsnop et al.* [1993] suggested that initial formation of metastable nitric acid dihydrate (NAD), or a ternary mixed hydrate of composition $HNO_3 \cdot H_2SO_4 \cdot 4H_2O$ (mixH) [*Fox et al.*, 1995], may provide the necessary nucleation step. These hydrates could eventually convert to NAT, bringing the system into a more stable thermodynamic equilibrium with the vapor phase. The PSC condensed phase also could be sulfate (H_2SO_4/H_2O) aerosols that take up H_2O and HNO_3 as they cool from 210 to 195 K, thereby forming a supercooled ternary solution (STS) of HNO_3, H_2SO_4, and H_2O [*Arnold*, 1992; *Hamill et al.*, 1988]. These droplets continue to take up additional H_2O and HNO_3 as temperatures approach the frost point [*Carslaw et al.*, 1994; *Tabazadeh et al.*, 1994a]. Frost-point temperatures may or may not lead to NAT nucleation out of the STS solution [*Molina et al.*, 1993; *Koop et al.*, 1995; *Iraci et al.*, 1995]. Comparing STS models to aerosol observations in the AASE data set, *Carslaw et al.* [1994], *Drdla et al.* [1994], and *Tabazadeh et al.* [1994b] demonstrate that STS composition provides better agreement than NAT for some conditions. From an analysis of Arctic cloud data, *Tabazadeh and Toon* [1996] also suggest that some aerosols are a dilute, metastable solid phase of HNO_3 and H_2O. In a reanalysis of infrared spectra taken in Antarctica in 1987, *Toon and Tolbert* [1995] concluded that the observed PSCs were not composed of NAT but were more consistent with STS. Although the field data sets have provided essential information describing the PSC aerosol, the understanding of PSC formation and composition remains incomplete.

During the recent Airborne Southern Hemisphere Ozone Experiment/Measurements for Assessing the Effects of Stratospheric Aircraft (ASHOE/MAESA) campaign, PSCs were observed during two flights of the NASA ER-2 high-altitude aircraft operating in the stratosphere near the edge of the Antarctic vortex in late July 1994. In addition to the concentration and size distribution of particles, measurements of NO_y, nitrous oxide (N_2O), pressure (P), and temperature (T) were made during the PSC encounter. Since there is only one other similar set of in situ observations in Antarctic PSCs [*Fahey et al.*, 1989a], these measurements represent an important expansion of data related to PSC composition and formation. Similarities between these recent observations and those made in the Arctic during AASE unify the discussion of PSCs for the two hemispheres and help to define the range of conditions and compositions that lead to PSC formation. However, some uncertainties remain regarding the nucleation and composition of these aerosols. In this paper, we present the new observations in a way that is consistent with earlier analyses [*Fahey et al.*, 1989a; *Kawa et al.*, 1992], using similar measurements and analysis tools. Three proposed compositions of the aerosol condensed phase are used in the analysis of these new observations: the NAT and NAD solid hydrates and the liquid STS. The equilibrium models of *Tabazadeh et al.* [1994a] and *Carslaw et al.* [1995a, b] are used for STS. The metastable solid solution [*Tabazadeh and Toon*, 1996] and the mixH [*Fox et al.*, 1995] are not addressed in this work.

The analysis here is limited to the PSC cloud event encountered on July 28, 1994. The criteria used to test each composition model include the prediction of the cloud onset and the abundance of condensed-phase HNO_3 in PSC aerosol along the flight track. The amount of condensed HNO_3 predicted by each model is compared with that inferred from aerosol and NO_y measurements. The results of this analysis show that the onset of the PSC is not collocated with NAT saturation conditions, nor does the NAT model adequately predict the abundance of HNO_3 in observed cloud particles. The results using the NAD model are similar. In contrast, the liquid STS model reproduces the transition to PSC particles and the abundance of HNO_3 in particles along the flight track extremely well. These results are substantially different than conclusions drawn from the AAOE data set, for which only NAT was actively considered. An additional comparison of modeled STS aerosol-size distributions with measured PSC aerosol-size distributions reveals good agreement at temperatures below 191 K. Two additional comparisons of the role of NAT and STS are made using the observations of July 28 as a basis. The first is a direct comparison of NAT and STS reactivities at ambient conditions. Finally, the NAT and STS models also are used to estimate the changes in observed PSC aerosol that would result when H_2O, HNO_3, and H_2SO_4 atmospheric mixing ratios are elevated by a fleet of high-speed civil transport (HSCT) aircraft.

Condensed-Phase Composition Models

The equilibrium partitioning of HNO_3 between the gas and the condensed phases can be estimated using models for both the variable composition of STS and the fixed composition of the frozen hydrates. For the frozen hydrates, an analytical expression describes the equilibrium vapor pressure of HNO_3

over the condensed phase. For STS composition, an iterative calculation using specified ambient conditions is required to find the composition of aerosols and the equilibrium vapor pressure of HNO_3. As discussed below, these equilibrium vapor pressures are essential for the three basic comparisons used to evaluate the composition of the observed PSC aerosol. Table 1 gives a brief definition of the terms and variables used in the model descriptions and in the following analyses and discussion.

NAT and NAD Saturation Mixing Ratios

For the solid hydrates NAT and NAD, the saturation or equilibrium mixing ratio of HNO_3 over the condensed phase ($[HNO_3]_{gas}^{NAT}$, $[HNO_3]_{gas}^{NAD}$) can be derived from the gas-solid

Table 1. Definitions of Terms and Variables

Term	Definition
$[NO_y]_{meas}$	total NO_y (ppbv) as measured from ER-2; in presence of PSC aerosols, NO_y is enhanced due to particle oversampling
Vol_{MASP}	total aerosol volume (μm^3 cm^{-3}) as measured by ER-2 MASP instrument
NO_y^*	surrogate for NO_y derived from NO_y-N_2O tracer relationship (equation (12))
$[HNO_3]_{gas}$	gas-phase mixing ratio of HNO_3 (not measured)
$[HNO_3]_{gas}^{NAT}$ $[HNO_3]_{gas}^{NAD}$	saturation mixing ratio of HNO_3 over NAT and NAD at ambient T, P, and H_2O (equations (1), (2), (3))
$[HNO_3]_{gas}^{STS}$	gas-phase mixing ratio of HNO_3 predicted by STS model
$[H_2O]_{sat}$	saturation mixing ratio of H_2O over water ice at ambient T and P
$[HNO_3]_{total}$	equivalent gas-phase mixing ratio of HNO_3 present in gas and condensed phases, assumed equal to $0.9[NO_y^*]$
$[H_2SO_4]_{total}$	equivalent gas-phase mixing ratio of H_2SO_4 present in gas and condensed phases, derived from FCAS aerosol measurements
$[H_2SO_4]_{cond}$	equivalent gas-phase mixing ratio of H_2SO_4 present in condensed phase; in STS model $[H_2SO_4]_{cond} = [H_2SO_4]_{total}$
$[H_2O]_{total}$	equivalent gas-phase mixing ratio of H_2O present in gas and condensed phases; estimated 4.8 to 5.0 ppmv, analyzed at 2.0, 3.0, 4.0, 5.0, and 6.0 ppmv
$[H_2O]_{gas}$	gas-phase mixing ratio of H_2O, approximately equal to $[H_2O]_{total}$ in STS model

Term	Definition
ρ_{STS}	STS aerosol density calculated as molality-weighted average of pure binary solution densities
$wt\%_{HNO_3}$	weight percent of HNO_3 in condensed phase
$wt\%_{H_2SO_4}$	weight percent of H_2SO_4 in condensed phase
$[HNO_3]_{MASP}$ $[HNO_3]_{MASP}^{NAT}$ $[HNO_3]_{MASP}^{NAD}$ $[HNO_3]_{MASP}^{STS}$	equivalent gas-phase mixing ratio of HNO_3 present in PSC particles derived from MASP volume measurements for a specific condensed phase (equations (17), (18), (19))
$[HNO_3]_{cond}$ $[HNO_3]_{cond}^{NAT}$ $[HNO_3]_{cond}^{NAD}$ $[HNO_3]_{cond}^{STS}$	equivalent gas-phase mixing ratio of HNO_3 present in PSC particles; equilibrium is assumed between gas and specific condensed phases (equation (13))
$[NO_y]_{aer}$ $[NO_y]_{aer}^{NAT}$ $[NO_y]_{aer}^{NAD}$ $[NO_y]_{aer}^{STS}$	equivalent gas-phase mixing ratio of NO_y incorporated into particles of a specific composition, derived from $[NO_y]_{meas}$ using enhancement of particles in NO_y sample inlet (equation (16))
S	saturation ratio
S_{NAT}	ratio of HNO_3 available to amount of HNO_3 that would be present at equilibrium with specific condensed phase; $S_{NAT} = 0.9[NO_y^*]/[HNO_3]_{gas}$ (equation (5))
S_{NAT}^{STS}	saturation ratio if HNO_3 is in equilibrium with the STS condensed phase; $S_{NAT}^{STS} = [HNO_3]_{gas}^{STS}/[HNO_3]_{gas}^{NAT}$
Vol_{STS}	total aerosol volume calculated from $[HNO_3]_{cond}^{STS}$ with perturbations to ambient H_2O, HNO_3, and H_2SO_4 according to Scenario IV of assessment (equation (20))
Vol_{NAT}	total aerosol volume calculated from $[HNO_3]_{cond}^{NAT}$ with perturbations to ambient H_2O and HNO_3 according to Scenario IV of assessment

equilibrium as a function of measured T, P, and H_2O. The NAT expression used in this analysis has been derived by *Hanson and Mauersberger* [1988] for temperatures between 180 and 200 K in the following form:

$$\log(P_{HNO_3}) = m(T)\log(P_{H_2O}) + b(T) \quad (1)$$

where

$$m(T) = -2.7836 - 0.00088(T),$$

$$b(T) = 38.9855 - \frac{11397.0}{T} + 0.009179(T),$$

P_{H_2O} is the ambient pressure of H_2O, P_{HNO_3} is the equilibrium pressure of HNO_3, T is in degrees Kelvin, P is in torr, and the uncertainty in P_{HNO_3} is about ±30%. $[HNO_3]_{gas}^{NAT}$ is derived by solving for P_{HNO_3} and converting to volume mixing ratio.

The saturation mixing ratio of NAD was derived using equilibrium constants as determined by *Smith* [1990] and *Worsnop et al.* [1993]:

$$[HNO_3 \cdot nH_2O]_{(s)} \leftrightarrow [HNO_3]_{(g)} + n[H_2O]_{(g)}$$

$$K_n = \left(P_{HNO_3}\right)\left(P_{H_2O}\right)^n \quad (2)$$

where $n = 2$ for NAD. This expression can be solved for P_{HNO_3} at different temperatures using the temperature-dependent expression for the equilibrium constant

$$\ln K_n = \frac{A}{T} + B \quad (3)$$

where

$$A = -\frac{\Delta H^\circ}{R},$$

$$B = \frac{\Delta S^\circ}{R} + 3\ \ln(760),$$

and K_n is in units of $(torr)^3$. For NAD, A = -22630 and B = 84.8 for the temperature range 180 to 210 K, with an uncertainty of about ±65% in P_{HNO_3}. A similar expression, derived for NAT, gives values of P_{HNO_3} that are virtually equivalent to the formulation expressed in (1) for stratospheric conditions.

The saturation ratio, S, is defined as the ratio of the ambient gas-phase mixing ratio of a particular species to the equilibrium mixing ratio over a condensed phase at ambient conditions. For example, S for NAT (S_{NAT}) is given by

$$S_{NAT} = \frac{[HNO_3]_{gas}}{[HNO_3]_{gas}^{NAT}} \quad (4)$$

where the differences from unity are a measure of how far the system is from equilibrium. To use S to examine the onset or edge features of a PSC where HNO_3 has not yet condensed into particles, the HNO_3 in the gas phase, $[HNO_3]_{gas}$, can be replaced with $[HNO_3]_{total}$, defined as the total available HNO_3 in the gas and condensed phases.

$$S_{NAT} \cong \frac{[HNO_3]_{total}}{[HNO_3]_{gas}^{NAT}} \cong \frac{0.9[NO_y^*]}{[HNO_3]_{gas}^{NAT}} \quad (5)$$

Furthermore, using a surrogate for NO_y derived from correlations with N_2O (NO_y^*, described below), $[HNO_3]_{total}$ can be approximated as $0.9[NO_y^*]$, since HNO_3 is expected to be ~90% of the NO_y reservoir from measurements at high latitudes [*Gao et al.*, 1997]. As HNO_3 condenses into particles, $0.9[NO_y^*]$ increasingly overestimates gas-phase HNO_3. NO_y^* also does not account for denitrified air in which NO_y has been irreversibly removed, or air into which NO_y has been redistributed by evaporation of settling particles [*Hübler et al.*, 1990].

Supercooled Ternary Solution (STS)

In this analysis the STS composition was determined primarily with the aerosol physical chemistry model (APCM) of *Tabazadeh et al.* [1994a], with comparisons to an analytic expression developed by *Carslaw et al.* [1995b]. The analytic expression is a parameterization of the comprehensive thermodynamic model for STS composition described by *Carslaw et al.* [1995a]. Valid for H_2O partial pressures between 2×10^{-5} and 2×10^{-3} mbar and temperatures between ~185 and 240 K, the analytic expression is appropriate to the conditions encountered during the flight of July 28, 1994. The two thermodynamic models (the APCM and the comprehensive model of *Carslaw et al.* [1995a]) are similar in that each must solve simultaneously equations describing the equilibrium between HNO_3 dissolved in the aerosol and in the gas phase and deriving ternary parameters from known binary solution parameters. Because of the variable composition of STS, both models use an iterative approach in determining the correct partitioning. However, the models differ in the way they express these quantities.

In the APCM, the equilibrium of HNO_3 between the gas and the condensed phases is expressed in terms of a mixed activity coefficient for HNO_3 in the ternary solution γ_{HNO_3},

$$HNO_{3(gas)} \leftrightarrow H^+_{(aq)} + NO^-_{3(aq)}$$

$$K_s(T) = \frac{m_{H^+} m_{NO_3^-} [\gamma^{mix}_{HNO_3}(T, m_S, m_N)]^2}{P_{HNO_3}} \quad (6)$$

where m is the molality of ions in solution, m_S is the molality of H_2SO_4, m_N is the molality of HNO_3, and P_{HNO_3} is the HNO_3 vapor pressure. The value of $\gamma^{mix}_{HNO_3}$ is derived as a combination of binary activities according to the empirical mixing rule of *Kusik and Meissner* [1978]:

$$\ln \gamma^{mix}_{HNO_3} = \frac{1}{2I}\left[2(m_N + m_S)\ln \gamma^{\circ}_{HNO_3}(T, I) + 2.25 m_S \ln \gamma^{\circ}_{H_2SO_4}(T, I)\right] \quad (7)$$

where $\gamma^{\circ}_{HNO_3}$ and $\gamma^{\circ}_{H_2SO_4}$ are the HNO_3 and H_2SO_4 mean activity coefficients in the binary H_2O/HNO_3 and H_2O/H_2SO_4 systems, respectively, evaluated at I, the ionic strength of the solution. This expression depends on measurements of HNO_3 vapor pressures over known STS compositions by *Zhang et al.* [1993].

In contrast, the thermodynamic model of *Carslaw et al.* [1995a] expresses the equilibrium of HNO_3 in terms of an effective Henry's law constant H^*.

$$P_{HNO_3} = \frac{m_N}{H^*} \quad (8)$$

H^* is dependent on the composition of the aerosol through m_N and m_S. H^* is calculated as a function of the Henry's law constants of HNO_3 in a binary HNO_3/H_2O solution (H^*_{NNb}) and a binary H_2SO_4/H_2O solution where HNO_3 is a trace species (H^*_{NSb})

$$H^* = \frac{H^*_{NNb}\, m_N}{(m_N + m_S)} + \frac{H^*_{NSb}\, m_S}{(m_N + m_S)}. \quad (9)$$

Both models use the Gibbs-Duhem relation for the condition of equilibrium. For STS this takes the form

$$\frac{m_S}{m^\circ_S} + \frac{m_N}{m^\circ_N} = 1 \quad (10)$$

where m°_S and m°_N are the pure binary molalities for H_2SO_4 and HNO_3, respectively, calculated at a given relative humidity. In the analytic expression, the binary solution parameters H^*_{NNb}, H^*_{NSb}, m°_S, and m°_N are fitted to the results of the *Carslaw et al.* [1995a] comprehensive model as simple expressions in terms of T and H_2O. Both models stipulate mass conservation such that

$$[HNO_3]_{total} = [HNO_3]^{STS}_{gas} + [HNO_3]^{STS}_{cond} \quad (11)$$

Similarly, both models assume that H_2SO_4 is present only in the aqueous phase and that any H_2O taken up by STS aerosols is negligible with respect to the gas phase, leaving the H_2O partial pressure constant during HNO_3 uptake. Both assumptions are valid for stratospheric conditions.

In both models, solving for the composition of STS requires inputs of H_2SO_4 mass, T, P, NO_y^*, and total H_2O, as well as the assumption that $[HNO_3]_{total}$ equals $0.9[NO_y^*]$. In applying this model to field data, available H_2SO_4 mass was obtained from aerosol measurements of particle concentration for sizes between 0.06 and 3.0 μm diameter as discussed below. For both the APCM and the analytic expression, the model output gives the equilibrium mixing ratio of HNO_3 in the gas phase ($[HNO_3]^{STS}_{gas}$), the equivalent gas-phase mixing ratio of HNO_3 in the condensed phase ($[HNO_3]^{STS}_{cond}$), and the weight percent of both HNO_3 and H_2SO_4 in the ternary solution ($wt\%_{HNO_3}$ and $wt\%_{H_2SO_4}$, respectively). The analytic expression also gives the STS density (ρ_{STS}), and the predicted STS aerosol volume. In the analytic expression, ρ_{STS} is calculated as the molality-weighted combination of the pure binary solution densities. For consistency this calculation of ρ_{STS} also is used in the APCM results.

Data and Derived Quantities

The data sets used in this analysis are NO_y, N_2O, hydrogen chloride (HCl), particle size and concentration, P, and T collected in situ from NASA's ER-2 high-altitude aircraft. Plate 1 displays some of these data sets, as well as some of the derived quantities for the ER-2 flight of July 28, 1994. The PSC was encountered at 64°S, 172.5°E, at an altitude of ~20 km on the southbound leg of a flight from Christchurch, New Zealand (44°S, 172.5°E). During the encounter the aircraft was inside the Antarctic polar vortex ~540 km poleward of the edge of the chemically perturbed region (CPR) (59°S), as defined by distinct changes in chlorine monoxide (ClO), NO_y, and N_2O. NO_y was measured using a gold catalytic converter to reduce NO_y species to NO, followed by detection of NO by nitric oxide/ozone (NO/O_3) chemiluminescence [*Fahey et al.*, 1989b; *Gao et al.*, 1997]. N_2O and HCl were measured using tunable diode laser spectroscopy [*Keim et al.*, this issue; *Webster et al.*, 1994].

A new Multiangle Aerosol Spectrometer Probe (MASP) provided the size and concentration for particle diameters of ~0.4 to 10.0 μm. MASP translates the light scattered by individual particles to a particle size using Mie scattering theory for spherical particles and an appropriate index of refraction [*Baumgardner et al.*, 1996]. MASP measurements of particle size and concentration are used to calculate the aerosol volume. Because MASP samples isokinetically, there is no loss of H_2O or HNO_3 from either sulfate or PSC particles. However, MASP measures only part of the ambient sulfate volume due to the 0.4-μm diameter lower size limit. Particle measurements from the Focused Cavity Aerosol Spectrometer (FCAS), which provides the size and concentration of particles in the 0.06- to 3.0-μm diameter size range [*Jonsson et al.*, 1995] were used to determine the total H_2SO_4 mass. Because of anisokinetic sampling, particles are compressionally heated in the FCAS inlet. As a result, the HNO_3 and much of the H_2O content of stratospheric sulfate aerosol are lost from particles before sizing. All FCAS data points are corrected by using the temperature-dependent deliquescence relationship for H_2SO_4/H_2O solutions developed by *Steele and Hamill* [1981] and ambient H_2O measurements to determine the ambient H_2SO_4 aerosol size and number distributions that would be present in the absence of ambient HNO_3 [*Jonsson et al.*, 1995]. Since the H_2SO_4 mass is unchanged in sampling, the FCAS measurements were used to calculate the H_2SO_4 content of both background and PSC aerosol. The H_2SO_4 mass contained in particles larger than the FCAS size limit of 3.0 μm is not included. However, for the flight of July 28, 1994, comparison of aerosol size distributions from the FCAS and MASP instruments indicates that the contribution to total aerosol volume from sizes greater than 3.0 μm is less than 1% inside the PSC, as well as along the rest of the flight track. In a comparison of the MASP and FCAS data sets in background aerosol outside the PSC, MASP aerosol volumes are ~35% larger than FCAS values, a difference that is within the combined error limits of both instruments (±60%). Therefore the error in the H_2SO_4 mass is estimated to be within ±60% for measurements inside the CPR.

The NAT and NAD saturation mixing ratios and the STS composition calculations require a measure of ambient H_2O. Although no measurements are available for the July 28 flight, successful data acquisition by the ER-2 Lyman-α H_2O instrument [*Kelly et al.*, 1989] prior to and following the PSC flight shows total H_2O to be rather constant along ER-2 flight tracks in the lower stratosphere poleward of Christchurch. The absence of significant dehydration in the successful July and August flights suggests that dehydrated air was unlikely to

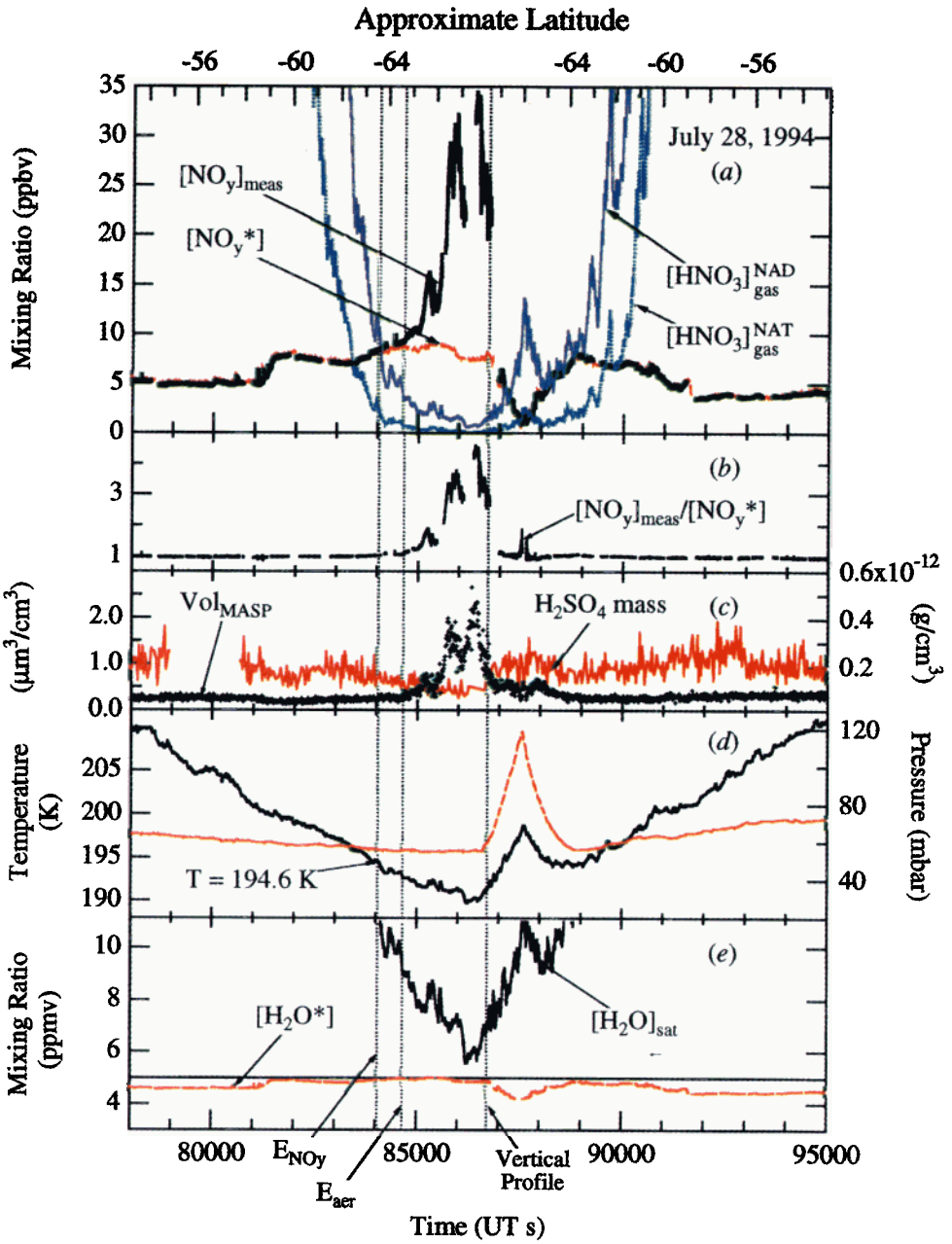

Plate 1. Time series of ER-2 data from the Antarctic flight of July 28, 1994. Approximate latitude along the flight track is given at the top. (a) Measured NO_y, the NO_y^* surrogate derived from measured N_2O, and the calculated saturation mixing ratios of HNO_3 over NAT and NAD ($[HNO_3]_{gas}^{NAT}$ and $[HNO_3]_{gas}^{NAD}$, respectively). (b) Ratio of $[NO_y]_{meas}$ to $[NO_y^*]$. (c) Total aerosol volume from Multiangle Aerosol Spectrometer Probe (MASP) measurements. (d) Measured T and P. (e) Saturation mixing ratio of H_2O over ice ($[H_2O]_{sat}$) and a surrogate for H_2O from measurements of N_2O (H_2O^*), with the line H_2O = 5.00 ppmv added for reference. Vertical dashed lines denote the first observation of NO_y enhancement (E_{NO_y} ~84000 UT s) and aerosol enhancement (E_{aer} ~84600 UT s), and the beginning of the aircraft vertical profile (~86700 UT s). Data for a 1-Hz sample rate are displayed where available; the MASP sample rate is 0.1 Hz.

have been sampled on the July 28 flight. The infrequent observations of dehydration throughout the ASHOE/MAESA mission are attributed to the limited vortex penetration achieved by the ER-2 and asymmetries in the transport of inner vortex air to the edge region [*Tuck et al.*, 1995; *Rosenlof et al.*, this issue]. Using the available H_2O data as well as the observed correlation of H_2O with N_2O on these same flights, total H_2O is estimated to be 4.8 to 5.0 parts per million by volume (ppmv) for the July 28 flight. The saturation mixing ratio for H_2O over ice ($[H_2O]_{sat}$), as calculated from T and P according to the *Smithsonian Institution* [1958] tables, suggests that ice aerosols probably do not contribute to the total

observed aerosol volume. Because of the absence of direct H_2O measurements, the sensitivity to the total H_2O estimate was examined in the analyses presented below by using integer values between 2 and 6 ppmv in separate calculations (see Appendix). With this H_2O estimate and the above measured parameters, derived quantities used in the analysis of PSC composition are presented below.

NOy*

Compact correlations of NO_y and N_2O observations in the lower stratosphere are commonly used to estimate a surrogate for total available NO_y from a measurement of N_2O [*Fahey et al.*, 1990]. This estimate, designated NO_y^*, is especially useful in regions of PSC activity where the presence of NO_y-containing particles leads to an enhancement of NO_y in the anisokinetic ER-2 sample inlet [*Fahey et al.*, 1989a], thereby increasing measured NO_y values above NO_y^*. In contrast, regions in which NO_y^* is greater than NO_y indicate that the sampled air has undergone denitrification, irreversibly removing NO_y through sedimentation of NO_y-containing particles. The evaporation of these particles can effect the redistribution of NO_y to lower altitudes, increasing total NO_y above NO_y^* calculated values [*Hübler et al.*, 1990]. Using data from four ASHOE/MAESA flights in late July/early August 1994, the linear correlation fit between NO_y and N_2O outside the polar vortex [*Keim et al.*, this issue] is given by

$$[NO_y^*] = 21.82 - 0.0699[N_2O] \quad (12)$$

where NO_y^* and N_2O are expressed in parts per billion by volume (ppbv). This expression, similar to previous evaluations [*Fahey et al.*, 1990], is used in the analysis here. The correlation is not altered significantly when data from within the polar vortex are included. However, data from air parcels that have been perturbed by denitrification or aerosol enhancement have not been included in the fit [*Keim et al.*, this issue].

Equilibrium-Condensed HNO_3

The equivalent gas-phase mixing ratio of the condensed HNO_3 ($[HNO_3]_{cond}$) in a PSC is estimated by assuming that the condensed phase is sampled at equilibrium. For all compositions, $[HNO_3]_{total}$ is assumed to be $0.9[NO_y^*]$. In the case of the solid hydrates, $[HNO_3]_{gas}$, calculated in equations (1) and (2), is the amount of HNO_3 present in the gas phase, where all remaining HNO_3 is assumed to be in the condensed phase. The result for NAT is given by

$$[HNO_3]_{cond}^{NAT} = 0.9[NO_y^*] - [HNO_3]_{gas}^{NAT} \quad (13)$$

An analogous expression defines $[HNO_3]_{cond}^{NAD}$. $[HNO_3]_{cond}^{STS}$ is calculated directly with the STS models that use $[HNO_3]_{total} = 0.9[NO_y^*]$ as an input condition.

NO_y Aerosol

NO_y is designated as the sum of the mixing ratios of reactive nitrogen species in the lower stratosphere, where HNO_3 is the principal component species. The remaining noncondensing fraction of NO_y in the polar lower stratosphere includes such species as NO, nitrogen dioxide (NO_2), nitrogen trioxide (NO_3), chlorine nitrate ($ClONO_2$), dinitrogen pentoxide (N_2O_5), nitrous acid (HONO), and peroxynitric acid (HO_2NO_2). As a result of ambient sample heating, the NO_y measurement includes volatile reactive nitrogen species contained in sampled particles. However, because of the difference between the inlet line flow velocity (15 m s^{-1}) and the true air speed of the aircraft (200 m s^{-1}), particles are oversampled, leading to an enhancement in the NO_y signal. As described above, this enhancement is evident in regions where NO_y is greater than NO_y^*. The sampling efficiency of the NO_y inlet for a given particle size is estimated by

$$A = \frac{1.68K + 0.13}{1.68K + 1.13}\frac{U_0}{U} + 2\frac{U}{U_0} \quad (14)$$

where U is the inlet flow velocity and U_0 is the true air speed of the aircraft [*Fahey et al.*, 1989a]. K is the Stokes parameter, expressed as

$$K = \frac{\rho D^2 C U_0}{18\mu_{air} d} \quad (15)$$

where ρ is the particle density, D is the particle diameter assuming that the shape is spherical, C is the Cunningham slip correction [*Pruppacher and Klett*, 1978], μ_{air} is the viscosity of air, and d is the inlet diameter. The uncertainty in A is estimated to be ±30%. The overall enhancement factor of the NO_y signal, A_{eff}, is the volume-weighted average of A calculated for particle sizes between 0.32 and 4.00 μm in diameter. Thus A_{eff} is a function of both the aerosol size distribution and the assumed particle composition. For the flight of July 28, NAT and NAD average A_{eff} values are 8.0 and 9.2, respectively, with highest values at coldest temperatures and larger aerosol sizes. For STS, the value of A_{eff} is more variable due to changes in ρ_{STS}, giving an average A_{eff} during the PSC encounter of 7.3.

Using A_{eff} and measured NO_y ($[NO_y]_{meas}$), the equivalent mixing ratio of NO_y incorporated into particles ($[NO_y]_{aer}$), can be estimated as

$$[NO_y]_{aer}^{NAT(NAD,STS)} = \frac{[NO_y]_{meas} - 0.1[NO_y^*] - [HNO_3]_{gas}^{NAT(NAD,STS)}}{A_{eff}} \quad (16)$$

where $0.1[NO_y^*]$ is the noncondensing fraction of available NO_y. A value of 0.1 is an estimate based on measured NO and calculated steady-state values of NO_2 and $ClONO_2$ as well as full-diurnal model results for the region outside the cloud for the July 30, 1994 flight [*Gao et al.*, 1997].

MASP HNO_3 Equivalent

The total volume (Vol_{MASP}) of particles during the PSC encounter is derived from MASP measurements of particle size and concentration. Using Vol_{MASP}, an equivalent volume mixing ratio of HNO_3 condensed in PSC particles ($[HNO_3]_{MASP}^{NAT}$, $[HNO_3]_{MASP}^{NAD}$, $[HNO_3]_{MASP}^{STS}$) can be calculated by assuming a respective composition for all aerosols. For NAT, which has a density of 1.62 g cm^{-3} and $wt\%_{HNO_3}$ of 53.8, the expression is

$$[HNO_3]_{MASP}^{NAT} = 1.15(Vol_{MASP})(T/P) \quad (17)$$

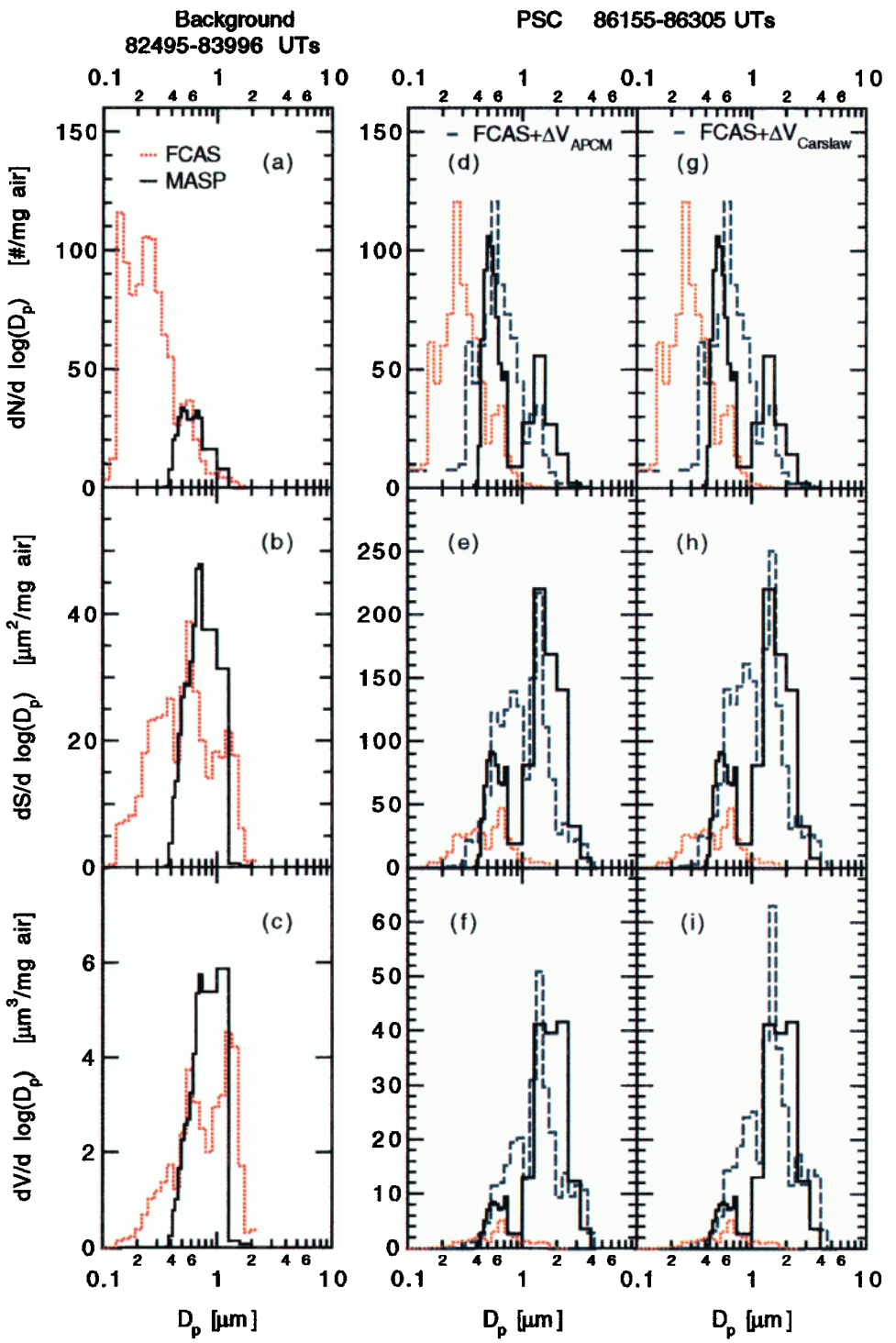

Plate 2. Average observed and calculated size distributions of aerosol particles for two periods along the flight track, where N, S, V, and D_p correspond to aerosol number, surface area, volume, and diameter, respectively. The three columns of size distributions show N, S, and V for sample periods in the background aerosol inside the chemically perturbed region (CPR) (Plates 2a-2c) and in the polar stratospheric cloud (PSC) aerosol for temperatures from 189.7 to 191.2 K (Plates 2d-2i). Observed size distributions are shown for the MASP (solid line) and Focused Cavity Aerosol Spectrometer (FCAS) (dotted line) instruments. The MASP instrument uses $\eta = 1.44$ for background samples and $\eta = 1.40$ inside the PSC. The simulations of MASP distributions from FCAS observations using (23), (24), and (25) for the APCM (Plates 2d-2f) and analytic expression (Plates 2g-2i) are shown with the dashed lines.

where T is in degrees Kelvin, P is in millibars, and Vol_{MASP} is in units of $\mu m^3\ cm^{-3}$. For NAD, a density of 1.70 g cm^{-3} was estimated from the average of the reported densities for NAT and nitric acid monohydrate (NAM) [*Taesler et al.*, 1975; *Delaplane et al.*, 1975]. This value is confirmed by a Lorentz-Lorenz analysis using the measured refractive index of NAD and molar refractivities for H_2O and HNO_3 determined by *Berland et al.* [1994] and *Middlebrook et al.* [1994]. Therefore, using the stoichiometric $wt\%_{HNO_3}$ value of 63.6, the result is

$$[HNO_3]^{NAD}_{MASP} = 1.43(Vol_{MASP})(T/P) \quad (18)$$

The assumption of a uniform HNO_3/H_2O composition of NAT or NAD for Vol_{MASP} over the entire flight track neglects the H_2SO_4 and H_2O mass associated with the background sulfate aerosol. Thus, outside the PSC where MASP samples only background aerosol volume, (17) and (18) overestimate the HNO_3 condensed mass. To a lesser extent, the same is true inside the PSC where the low vapor pressure of H_2SO_4 causes it to remain in the condensed phase as PSCs grow, regardless of the PSC composition. To account for this overestimate, the average Vol_{MASP} value for the first 1000 s of flight track just inside the CPR but outside the PSC was subtracted from all Vol_{MASP} values before $[HNO_3]_{MASP}$ was calculated for the NAT and NAD compositions. In this way, $[HNO_3]^{NAT}_{MASP}$ and $[HNO_3]^{NAD}_{MASP}$ are reduced by 0.2 and 0.4 ppbv, respectively, giving values near zero in regions of background aerosol volume.

Since measured STS densities for a range of compositions are not available, ρ_{STS} at any point along the flight track is approximated for both the APCM and the analytic expression as the molality-weighted combination of the pure binary solution densities. Therefore the equivalent gas-phase mixing ratio of HNO_3 in STS depends on density and weight percent as

$$[HNO_3]^{STS}_{MASP} = 1.32(10^{-2})(\rho_{STS})(wt\%_{HNO_3})(Vol_{MASP})(T/P) \quad (19)$$

For the July 28 flight, two different refractive indices were used in the MASP size calculation. The first value (η = 1.44) is comparable to the refractive indices of aerosols containing concentrated H_2SO_4, NAT, or NAD. The second value (η = 1.40) is an estimate of the value for STS reflecting a larger H_2O content than the other compositions. The use of the lower refractive index resulted in a 30% average increase in measured aerosol volume inside the cloud.

In the calculation of Vol_{MASP}, only aerosols between 0.32 and 4.00 μm in diameter are used to be consistent with calculations of $[NO_y]_{aer}$. The nature of the anisokinetic inlet of the NO_y instrument is such that particles larger than 4.00 μm are inertially separated from the sample stream and therefore produce no NO_y signal [*Fahey et al.*, 1989a]. The additional volume associated with particles larger than 4.00 μm in the MASP size distribution is less than 1%.

Comparison of Derived Quantities

The models for condensed-phase composition and the range of derived quantities described above allow specific comparisons that address the composition of PSC aerosol particles. Three basic comparisons using the onset and equilibrium abundance criteria of condensed-phase HNO_3 are listed in Table 2. Both criteria relate to a time series of PSC observations obtained along the aircraft flight track. The onset of the PSC or transition to PSC aerosol refers to the location along the flight track where condensed-phase HNO_3 becomes a significant fraction of the ambient aerosol. As shown below, this criterion is more difficult to define for the STS composition than for the frozen hydrates because the modeled transition to PSC aerosol is more gradual and its detection is limited by instrumental sensitivities. The second criterion refers to the relative and absolute abundance of condensed-phase HNO_3 predicted within a PSC.

In previous analyses [*Fahey et al.*, 1989a; *Kawa et al.*, 1992] the cloud onset was tested by comparing the region of NAT saturation to that where aerosols were enhanced above background values. The region of NAT saturation was defined using the saturation mixing ratio of HNO_3 over NAT ($[HNO_3]_{HM}$ and $[HNO_3]_s$ in the two analyses, respectively) and total available HNO_3. In this analysis a similar test of cloud onset is made for both NAT and NAD using their respective saturation mixing ratios, $[HNO_3]^{NAT}_{gas}$ and $[HNO_3]^{NAD}_{gas}$, and $[NO_y^*]$ to estimate total HNO_3 (Table 2, comparison A). Unlike the frozen hydrates, the variable STS composition involves an additional dependence on $[HNO_3]_{total}$ that leads to calculated HNO_3 gas-phase mixing ratios which are necessarily consistent with the STS condensed phase. Therefore comparison A with the criterion of PSC onset is not made for STS composition.

For the criterion of the abundance of condensed HNO_3, $[HNO_3]_{MASP}$ inferred from the aerosol measurements is compared with $[HNO_3]_{cond}$ from one of the composition models (Table 2, comparison B), or with $[NO_y]_{aer}$ (Table 2, comparison C) inferred from NO_y measurements, thereby providing two independent tests of that model. Comparison B in Table 2 allows a test of how well a given model reproduces the absolute value and variations in the abundance of $[HNO_3]_{MASP}$ along the flight track, in addition to the location of the cloud onset. As such, this comparison is the only one to use both criteria. However, this test of abundance is invalidated when total NO_y has been perturbed by denitrification or redistribution. An additional comparison of $[HNO_3]_{cond}$ and $[NO_y]_{aer}$ could be made using both criteria. However, because of the larger error associated with $[NO_y]_{aer}$ (see Appendix), the test of composition would be less certain. Instead $[NO_y]_{aer}$ is used in comparison with $[HNO_3]_{MASP}$ (Table 2, comparison C) as a test for consistent agreement between measurements of enhanced NO_y and aerosol and the predictions of a given composition model. Because both $[HNO_3]_{MASP}$ and $[NO_y]_{aer}$ are derived from measurements (NO_y and aerosol, respectively), this abundance comparison is unaffected by perturbations such as denitrification and redistribution.

ASHOE/MAESA Antarctic Results

The flight track observations and derived quantities for the flight of July 28 are shown in part in Plate 1. The region of PSC activity addressed in this analysis begins at the cloud

Table 2. Comparisons Made to Test Edge and Intensity Features of PSC Activity

	Comparison	Onset[a]	Abundance[a]	Notes
A	$\{[NO_y^*] > [HNO_3]_{gas}^{NAT}\}$ versus E_{NO_y}, E_{aer} $\{[NO_y^*] > [HNO_3]_{gas}^{NAD}\}$ versus E_{NO_y}, E_{aer}	√	N/A	$\{NO_y^* > [HNO_3]_{gas}\}$ defines region in which saturation conditions exist no comparison is made for STS model (Plate 1) E_{NO_y} denotes first occurrence of NO_y enhancement on poleward leg of flight track; E_{aer} denotes aerosol enhancement
B	$[HNO_3]_{cond}^{NAT}$ versus $[HNO_3]_{MASP}^{NAT}$ $[HNO_3]_{cond}^{NAD}$ versus $[HNO_3]_{MASP}^{NAD}$ $[HNO_3]_{cond}^{STS}$ versus $[HNO_3]_{MASP}^{STS}$	√	√	makes assumption that total available NO_y is equal to $[NO_y^*]$ comparison of absolute abundance will be degraded by denitrification or redistribution (Figure 1)
C	$[NO_y]_{aer}^{NAT}$ versus $[HNO_3]_{MASP}^{NAT}$ $[NO_y]_{aer}^{NAD}$ versus $[HNO_3]_{MASP}^{NAD}$ $[NO_y]_{aer}^{STS}$ versus $[HNO_3]_{MASP}^{STS}$	√	√	makes no assumption of total NO_y available for condensation; tests consistency of NO_y and MASP aerosol measurements with respect to given composition correlations in relative abundance reflect correlations in source measurements but do not reflect agreement with specific model (Figure 2)

[a]A (√) denotes a meaningful test using the specific comparison of derived quantities; N/A, not applicable.

onset near 84000 UT s and ends where the aircraft begins its vertical profile at ~86700 UT s (vertical dashed lines labeled "E_{NO_y}" and "vertical profile" in Plate 1). The onset of the cloud, the point at which $[NO_y]_{meas}$ and NO_y^* diverge (Plate 1b), occurs during this flight as temperatures fall below 194.6 K (Plate 1d). NO_y enhancement indicates incorporation of HNO_3 in the observed aerosol, distinguishing it from background sulfate aerosol. During the time period from 84000 to 86700 UT s, which corresponds to a distance of ~540 km or 3.5° latitude, ambient pressures are near 60 mbar (19.5 km altitude) and ambient temperatures are between 189 K and 196 K (Plate 1d), decreasing fairly linearly with time. Gaps in the time series of NO_y measurements are due to instrument calibration checks. The region beyond 86700 UT s is neglected in this analysis because the PSC activity is significantly weaker and because the region includes the aircraft vertical profile during which ambient conditions are changing rapidly, thereby increasing the uncertainty in both measurements and models. The PSC region also is defined by values of Vol_{MASP} that exceed background values of ~0.3 μm^3 cm^{-3} (Plate 1c). *Dye et al.* [1996] also have used significant increases in aerosol volume to reference the onset of the PSC. Significant increases in MASP aerosol volume are not apparent along the flight track until ~122 km beyond E_{NO_y} at a temperature of 192.9 K. The reference line for aerosol enhancement also is noted in Plate 1 as a vertical dashed line (E_{aer}). This difference in apparent onset of the PSC between E_{NO_y} and E_{aer} locations is more related to assessing small differences in the time series of measurements than to a physical feature of the observed aerosol. As in previous analyses, the correlation between Vol_{MASP} and $[NO_y]_{meas}/[NO_y^*]$ values provides strong evidence that the observed aerosols contain reactive nitrogen species in the condensed phase. Moreover, Type II (water ice) PSCs cannot be the source of increased aerosol volume because $[H_2O]_{sat}$ exceeds the estimate of ambient H_2O ($[H_2O^*]$ from the H_2O/N_2O correlation) throughout the PSC region (Plate 1e). Minimum values of $[H_2O]_{sat}$ are 6 ppmv, whereas ambient H_2O values for this flight are estimated to be closer to 4.9 ppmv. Minimum $[H_2O]_{sat}$ values of 4 ppmv would require a decrease in minimum temperature of 2 K. The redistribution of H_2O into or out of the sampled air parcels is not considered here.

The distribution of aerosol number density, surface area, and volume measured by the FCAS and the MASP instruments in background aerosol and in PSC aerosol are shown in Plate 2. In the background the aerosol number densities for the two instruments show good agreement for diameters between 0.5 to 2.0 μm (the overlap of particle size range in the two instruments) (Plate 2a). Differences noted in number density are accentuated in the distributions of surface area and volume (Plates 2b and 2c, respectively) due to the dependence on particle diameter. In volume, MASP values are ~35% larger than FCAS values in the overlapping size range. Inside the PSC (Plates 2d-2i), discrepancies are larger due to the different sampling characteristics of the two instruments. As discussed above, MASP measures PSC particles without the loss of volatile components, while FCAS effectively measures the back-

ground aerosol because of the loss of condensed HNO_3 upon sampling. The advantage of this sampling difference is that it provides a consistent measurement of both available H_2SO_4 and total aerosol volume inside a PSC.

In the FCAS background aerosol, the median size increases from ~0.2 μm in the number distribution (Plate 2a) to ~0.8 μm in the volume distribution (Plate 2c). Inside the PSC the effective number distribution of "binary" aerosols (FCAS-dotted line, Plates 2d, 2g) is shifted to somewhat larger sizes. This shift is probably due to the low temperatures in this flight track region ($T < 191$K) that cause even binary sulfate aerosols to increase in size through H_2O uptake. The MASP measurements in Plate 2 (solid line) clearly show the presence of larger particles associated with PSC formation. The median sizes in the volume distributions increase to over 1 μm inside the PSC (Plates 2f, 2i). Volume distributions in Arctic PSCs measured with a comparable instrument showed similar size and concentration values [*Dye et al.*, 1992]. The size of the observed PSC aerosols further indicates the absence of ice aerosols, which should grow to much larger sizes due to the greater H_2O abundance. For PSC measurements shown in Plate 2, the areas of the number distribution for both MASP and FCAS are comparable, indicating that a significant fraction of available background aerosol particles participate in the growth of the PSC.

The saturation mixing ratios $[HNO_3]_{gas}^{NAT}$ and $[HNO_3]_{gas}^{NAD}$ in Plate 1a can be used to approximate regions of particle saturation ($[NO_y^*] > [HNO_3]_{gas}$) that would be expected for a condensed phase at equilibrium (Table 2, comparison A) [*Fahey et al.*, 1989a]. The NAT saturation region exceeds that of enhanced particle volume (E_{aer}) and NO_y (E_{NO_y}), consistent with previous analyses of Arctic PSCs [*Kawa et al.*, 1992; *Dye et al.*, 1992]. In contrast, the predicted onset of NAD aerosol ($[NO_y^*] > [HNO_3]_{gas}^{NAD}$) is in much better agreement with E_{NO_y} in Plate 1a than is the predicted onset of NAT aerosol. As described by *Worsnop et al.* [1993], a high free-energy barrier for nucleation of NAT might lead instead to the nucleation of NAD, a relatively persistent metastable phase. Metastable phases are expected to be less ordered and to have lower surface free energies and therefore have less of a barrier to nucleation. For example, *Disselkamp et al.* [1996] have found the interfacial surface energy of NAD to be 22 erg cm^{-2}, compared with 44 erg cm^{-2} previously estimated for NAT.

$[HNO_3]_{cond}$ and $[HNO_3]_{MASP}$ are compared for each composition in Figure 1 (Table 2, comparison B). The magnitude of $[HNO_3]_{MASP}$ varies with composition because of differences in density and $wt\%_{HNO_3}$, with lowest $[HNO_3]_{MASP}$ values for STS and highest for NAD. While the NAT and NAD equilibria require $[HNO_3]_{MASP}$ to be between 8 and 10 ppbv at the lowest observed temperatures, STS requires only around 6 ppbv. The time series of values for each composition display the same qualitative features since each is derived from aerosol measurements. Thus, in all cases, $[HNO_3]_{MASP}$ displays the same gradual increase at the onset of the cloud seen in Vol_{MASP} (Plate 1c).

The values of $[HNO_3]_{cond}$ for the frozen hydrates NAT and NAD display a threshold behavior as a function of ambient temperature (Figures 1e, 1f) and as a function of time (Figures 1b, 1c) because of uniformly decreasing temperatures (Plate 1d). Threshold behavior occurs because, once the saturation temperature is reached, further small decreases in temperature cause significantly more HNO_3 to be sequestered in particles. For temperatures at and below ~192 K, comparing $[HNO_3]_{cond}^{NAT}$ ($[HNO_3]_{cond}^{NAD}$) with $[HNO_3]_{total}$ indicates that virtually all available HNO_3 is condensed in the NAT (NAD) phase at equilibrium (Figures 1e, 1f). Thus the large variations in $[HNO_3]_{MASP}$ that occur at these temperatures, reflecting the actual abundance of HNO_3 in the condensed phase, are inconsistent with predicted $[HNO_3]_{cond}$ values. A further inconsistency is that values of $[HNO_3]_{MASP}$ exceed those of $[HNO_3]_{total}$ for both NAT and NAD at the lowest observed temperatures, thereby requiring that more HNO_3 be in the condensed phase than is apparently available. Figure 1 also shows that the earlier thresholds for both NAT and NAD are reached well outside the region of enhanced aerosol. Although the existence of a nucleation barrier for either NAT or NAD could serve to move these thresholds to later times and lower temperatures, the characteristic threshold behavior would still be expected. Because of this threshold behavior, neither the NAT nor the NAD models can adequately represent the variations of $[HNO_3]_{MASP}$ along the flight track.

In contrast to NAT and NAD, the modeled abundance of condensed HNO_3 in the STS PSC is dependent on the solubility of HNO_3 in the liquid H_2SO_4/H_2O aerosol phase. The model results for $[HNO_3]_{cond}^{STS}$ are in better agreement with $[HNO_3]_{MASP}^{STS}$ (Figures 1a, 1b), with the former displaying a more gradual increase with time along the flight track rather than a threshold response. Although $[HNO_3]_{cond}^{STS}$ is less than $[HNO_3]_{MASP}^{STS}$ throughout the entire PSC, relative changes in $[HNO_3]_{cond}^{STS}$ are well correlated with those of $[HNO_3]_{MASP}^{STS}$, and better and more consistent agreement of the absolute values is found. Observed differences are more easily accounted for by experimental uncertainties than the differences noted for NAT and NAD. For example, a simple scaling of the MASP volume results could significantly improve agreement for STS in Figure 1 but not for NAT or NAD.

An important feature of the STS model results in Figure 1 is the gradual increase in $[HNO_3]_{cond}$ with decreasing temperature and the favorable comparison with $[HNO_3]_{MASP}$. In contrast, the NAT and NAD models show a threshold response as discussed above, with large increases in $[HNO_3]_{cond}$ occurring after the saturation temperature is reached. The gradual increase of STS occurs because the composition of STS is a function of temperature, as shown in Plate 3c. At the threshold temperatures of NAT and NAD, $wt\%_{HNO_3}$ values for STS remain less than 10%. Maximum STS values of 40% are observed at the lowest temperatures in the PSC and are closer to the fixed NAT and NAD values (53.8% and 63.6%, respectively).

Other important facets of STS composition are highlighted in Plate 3c. First, $wt\%_{H_2O}$ does not change significantly over the temperature range of the PSC (190 to 200 K), varying only between 45 and 55%. In contrast, $wt\%_{HNO_3}$ and $wt\%_{H_2SO_4}$ display significant anticorrelated fluctuations for the same conditions, with $wt\%_{HNO_3}$ reaching values as high as 40 and $wt\%_{H_2SO_4}$ reaching values as low as 6 at 190 K. Values of $wt\%_{HNO_3}$ and $wt\%_{H_2SO_4}$ are multivalued in temperature due to

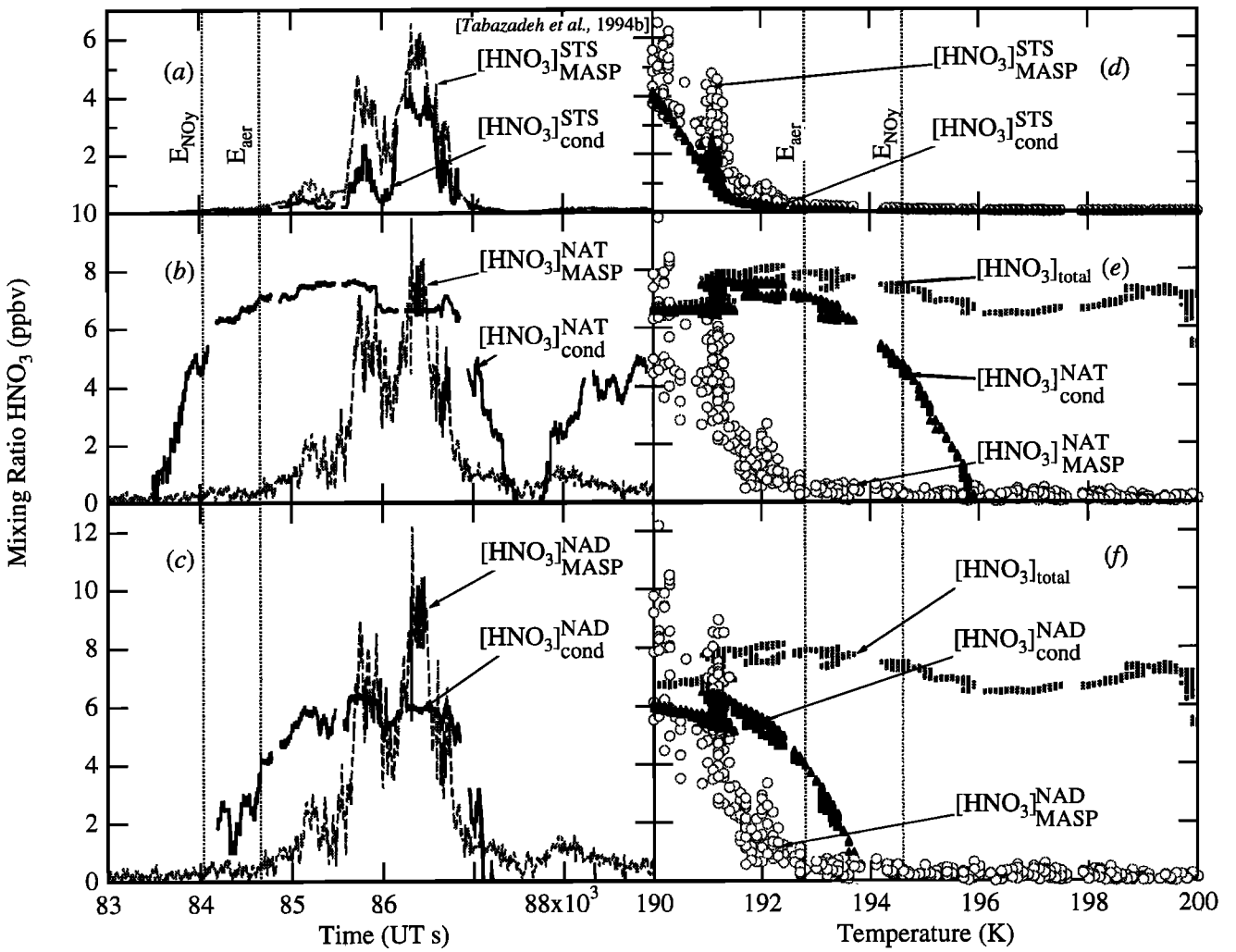

Figure 1. Comparison of equivalent gas-phase mixing ratios of condensed-phase HNO_3 derived from aerosol measurements ($[HNO_3]_{MASP}$) and from the equilibrium model ($[HNO_3]_{cond}$) for different aerosol compositions (Table 2, comparison B). Also shown for NAT and NAD is $[HNO_3]_{total}$. Data in panels on the left are displayed as a time series along the flight track, while data on the right are displayed as a function of temperature for the poleward portion of the flight (UT < 86700 s). Supercooled ternary solution (STS), NAT, and NAD (top, middle, and bottom) are used in the comparisons. $[HNO_3]_{MASP}$ is calculated for a 0.1-Hz sample rate, while $[HNO_3]_{cond}$ and $[HNO_3]_{total}$ are calculated for a 1-Hz sample rate. Vertical dashed lines for NO_y enhancement (E_{NO_y}) and aerosol enhancement (E_{aer}) define the region of transition into the PSC on the poleward leg of the flight track.

fluctuations in ambient NO_y and H_2SO_4. These changes in composition, corresponding to changes in the water activity in solution (a_{H_2O}), have a strong impact on the heterogeneous reactivity of STS aerosols.

The comparison of $[HNO_3]_{MASP}$ with $[NO_y]_{aer}$ (Table 2, comparison C) for each of the compositions is displayed in Figure 2, where $[HNO_3]_{MASP}$ is the same as shown in Figure 1. Because $[NO_y]_{aer}$ varies with composition due to the dependence of A_{eff} on particle density, the highest values occur with an assumed composition of STS and lowest values with NAD. The relative magnitudes of $[HNO_3]_{MASP}$ and $[NO_y]_{aer}$ are well correlated in each case because they are derived from Vol_{MASP} and $[NO_y]_{meas}$, respectively, which also are well correlated (Plates 1a, 1c). For all three compositions, $[NO_y]_{aer}$ is less than $[HNO_3]_{MASP}$. With NAT, $[NO_y]_{aer}$ underpredicts $[HNO_3]_{MASP}$ by about a factor of 2, while with NAD the difference is closer to a factor of 3. With STS, $[HNO_3]_{MASP}$ is underpredicted by ~50%. Although the combined uncertainties are comparable to the observed differences, the STS model provides significantly more consistent results as in comparison B.

A similar analysis of STS composition was performed using the analytic expression developed by *Carslaw et al.* [1995b]. The results of these model calculations are compared with those from the APCM of *Tabazadeh et al.* [1994b] in Plate 3. The quantities $[HNO_3]^{STS}_{cond}$, $[HNO_3]^{STS}_{MASP}$, and $[NO_y]^{STS}_{aer}$ are combined for the APCM in Plate 3a (also Figures 1a and 2a) and for the Carslaw analytic expression in Plate 3b. The agreement between $[HNO_3]^{STS}_{cond}$ and $[HNO_3]^{STS}_{MASP}$ is significantly improved with the Carslaw expression.

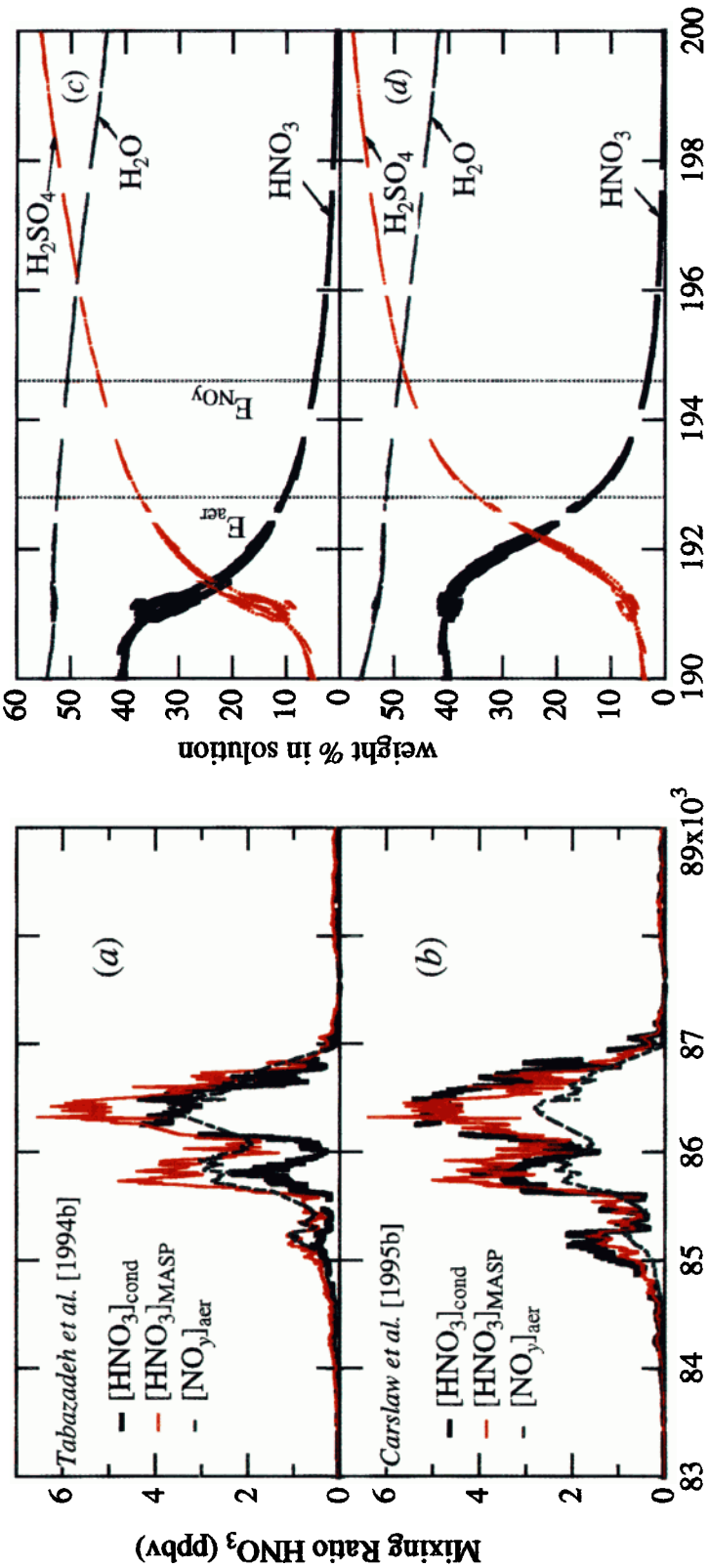

Plate 3. Comparison of STS composition calculations from the aerosol physical chemistry model (APCM) of *Tabazadeh et al.* [1994b] (a, c) with those from the analytic expression of *Carslaw et al.* [1995b] (b, d). Data in panels on the left are displayed as a time series along the flight track, while data on the right are displayed as a function of temperature for the poleward portion of the flight (UT < 86700 s). Plates 3a and 3b display the three values of condensed-phase HNO_3 ($[HNO_3]_{cond}$, $[HNO_3]_{MASP}$, and $[NO_y]_{aer}$) calculated independently for each model, while Plates 3c and 3d display the corresponding $wt\%_{HNO_3}$, $wt\%_{H_2SO_4}$, and $wt\%_{H_2O}$ for each model. Data are calculated for a 0.1-Hz sample rate. Vertical dashed lines for NO_y enhancement (E_{NO_y}) and aerosol enhancement (E_{aer}) define the region of transition into the PSC on the poleward leg of the flight track.

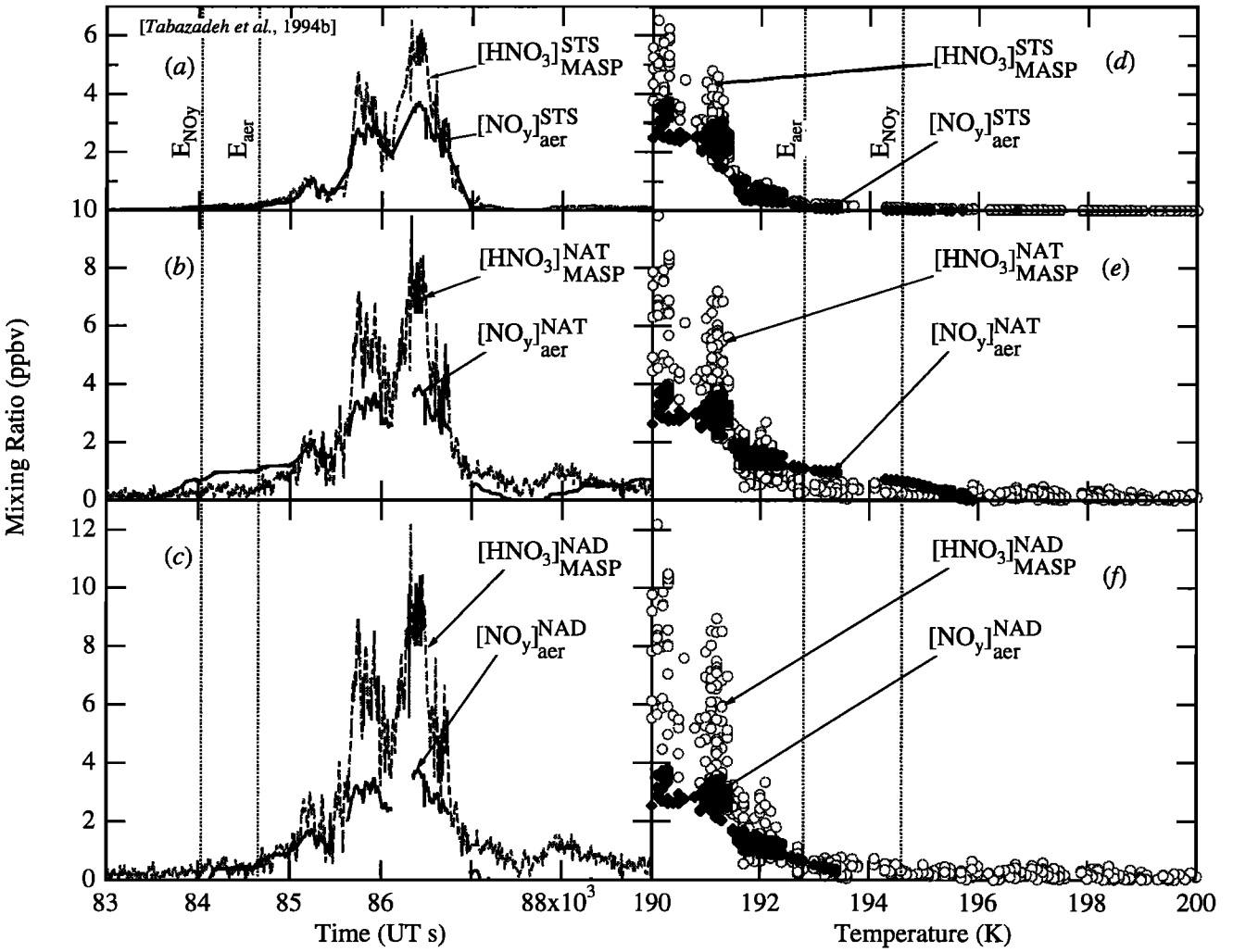

Figure 2. Comparison of $[HNO_3]_{MASP}$ and $[NO_y]_{aer}$ derived from MASP aerosol measurements and measured NO_y, respectively (Table 2, comparison C). Panels on the left display results as a time series along the flight track, while panels on the right display results as a function of temperature for the poleward portion of the flight (UT < 86700 s). STS, NAT, and NAD (top, middle, and bottom) are used in the comparisons. Both $[HNO_3]_{MASP}$ and $[NO_y]_{aer}$ are calculated for a sample rate of 0.1 Hz. Vertical dashed lines for NO_y enhancement (E_{NO_y}) and aerosol enhancement (E_{aer}) define the region of transition into the PSC on the poleward leg of the flight track.

However, the comparison between $[HNO_3]^{STS}_{MASP}$ and $[NO_y]^{STS}_{aer}$ is degraded from that made with the APCM. Both $[HNO_3]^{STS}_{MASP}$ and $[NO_y]^{STS}_{aer}$ values are different for the analytic expression because of differences in the predicted composition of STS between the two models. A change in composition leads to different values of ρ_{STS}. As a result, $[HNO_3]_{MASP}$ and A_{eff} ($[NO_y]_{aer}$) are increased (reduced) relative to the APCM, giving discrepancies between $[HNO_3]^{STS}_{MASP}$ and $[NO_y]^{STS}_{aer}$ of a factor of ~2 as found in the NAT comparison. Another difference between these two models is the value of $wt\%_{HNO_3}$ and $wt\%_{H_2SO_4}$ for a given set of ambient conditions, as shown in Plates 3c and 3d. Although there are significant differences for $wt\%_{HNO_3}$ inside the PSC, both models show 10% HNO_3 in the region along the flight track that corresponds approximately to the transition to enhanced aerosol volume. Although $wt\%_{HNO_3}$ rarely exceeds 40% in either model, the Carslaw result reaches 40% HNO_3 for temperatures almost a degree higher than the APCM but shows little change for further decreases in T. The differences between the two STS models are a reflection of some of the uncertainties in the prediction of STS composition at low temperatures. However, the predictions of both models are more consistent with the observations than either the NAT or the NAD models.

As noted above, all three composition models are sensitive to changes in ambient H_2O mixing ratios. The quantities shown in Figures 1 and 2 and Plate 3 are calculated with an H_2O value of 5.0 ppmv. H_2O values must be reduced to 3.0 ppmv (2.0 ppmv) for NAD (NAT) to eliminate regions of supersaturation. However, at these H_2O values, $[HNO_3]_{cond}$ underpredicts $[HNO_3]_{MASP}$ by ~80% and ~70% for NAD and NAT, respectively, and values of $[NO_y]_{aer}$ are even lower. The STS results display a similar sensitivity to changes in ambient H_2O. However, the sensitivity of $[HNO_3]^{STS}_{cond}$ to changing H_2O is accompanied by changes in $wt\%_{HNO_3}$ and ρ_{STS}, leaving the relative abundance of $[HNO_3]^{STS}_{cond}$ in good agreement with $[HNO_3]^{STS}_{MASP}$ and $[NO_y]^{STS}_{aer}$ for H_2O values between 4.0 and 6.0

ppmv. Below 4.0 ppmv H_2O the PSC is not apparent in the STS model. The H_2O sensitivity of the three models is described in more detail in the Appendix.

In summary, comparison A in Table 2 reveals that the region of NAD saturation corresponds more closely to the region of enhanced aerosol than the region of NAT saturation. Comparison B in Table 2 of condensed HNO_3 predicted for NAD at equilibrium ($[HNO_3]^{NAD}_{cond}$) with observed aerosol volume ($[HNO_3]^{NAD}_{MASP}$) also reveals that NAD more closely represents the observed onset of the cloud than NAT. However, the NAT and NAD frozen hydrate results both reveal that large regions of the flight track are supersaturated and both display a threshold behavior that is not reflected in the aerosol or NO_y observations. The absence of threshold behavior in the aerosol observations suggests that, despite the slightly better agreement for NAD, the observed aerosol volume is unlikely to be either hydrate phase. In contrast, comparison B shows consistent agreement between the two STS equilibrium models and quantities derived from observed aerosol. STS composition also leads to more consistent agreement between calculated values of $[NO_y]_{aer}$ and $[HNO_3]_{MASP}$ (derived from measurements of NO_y and aerosol, respectively) than NAT or NAD. Thus, despite some remaining discrepancies in these comparisons, STS composition best represents the PSC observations of the July 28 flight.

Discussion

The results in Figures 1 and 2 show that an STS equilibrium composition provides the most consistent comparison with quantities derived from observations. Before considering the relative roles of STS and NAT aerosol for reactivity and atmospheric perturbations, we first examine the relative errors in the current analysis, the importance of the equilibrium assumption, the formation of NAD and NAT in the presence of STS, and the consistency of the current analysis with those made earlier using Arctic and Antarctic observations.

Uncertainties

While the weight of evidence clearly rests with STS composition, neither NAT nor NAD composition can be completely ruled out based on the observations of the PSC encountered on July 28. As in the Arctic analysis described below, the apparent inconsistency between absolute values of $[HNO_3]^{NAT}_{MASP}$ and $[HNO_3]^{NAT}_{cond}$ in Figure 1 is encompassed by overlapping instrumental and model uncertainty limits at about the 1-σ confidence level (±60% in $[HNO_3]^{NAT}_{MASP}$ and ±43% in $[HNO_3]^{NAT}_{cond}$) if the HNO_3 fraction of NO_y is ~0.9. Because of the larger error in $[HNO_3]^{NAD}_{MASP}$ due to the large uncertainty in the density of NAD, the discrepancy in the comparison of $[HNO_3]^{NAD}_{MASP}$ with $[HNO_3]^{NAD}_{cond}$ also falls well within the error of the measurements (±65% in $[HNO_3]^{NAD}_{MASP}$ and ±73% in $[HNO_3]^{NAD}_{cond}$). In contrast, $[HNO_3]^{STS}_{MASP}$ represents up to 80% of the HNO_3 available, a fraction that not only is well within the error of the measurements but also is a reasonable fraction of NO_y*.

With respect to the general discrepancy between $[HNO_3]^{NAT,NAD}_{MASP}$ and $[HNO_3]_{total}$, a contribution from the denitrification and/or redistribution of NO_y prior to observation by the ER-2 cannot be ruled out. However, since $[HNO_3]_{MASP}$ and $[NO_y]_{aer}$ are both quantities derived from measurements, they are unaffected by denitrification and redistribution. The lack of agreement in this latter comparison for NAT and NAD compositions is an indication that these changes to total NO_y cannot completely account for the discrepancy.

Modeled STS Size Distributions

A further test of STS composition can be made by modeling the number, surface, and volume distributions of STS aerosol particles in the PSC peaks (Plate 1c) using FCAS observations and comparing these distributions to the MASP observations. As described above, the FCAS distributions are calculated using the assumption that only binary H_2SO_4/H_2O aerosols are present since neglecting the HNO_3 component is a good approximation everywhere outside of a PSC. To compare FCAS distributions with those of MASP inside a PSC, the HNO_3 lost from the FCAS-sampled aerosols must be calculated and added back to each distribution. Using the STS composition model to calculate the abundance of lost HNO_3 provides a unique test of the model. The total aerosol volume predicted by the STS model at equilibrium can be obtained in the PSC peaks by using an equation similar to (19):

$$\mathrm{Vol}_{STS} = \frac{[HNO_3]^{STS}_{cond}(P)}{1.3186(10^{-2})(\rho_{STS})(\mathrm{wt\%}_{HNO_3})(T)} \quad (20)$$

where $[HNO_3]^{STS}_{cond}$ from an STS model is used in place of $[HNO_3]^{STS}_{MASP}$. To predict the MASP distributions, the STS volume calculated to be present in excess of the FCAS-measured volume must be partitioned among particles in the observed FCAS size distribution. This in effect converts the aerosol represented by the FCAS distributions from "binary" to "ternary."

With the assumption that both FCAS and MASP are measuring aerosols at equilibrium and because both aerosol measurements are made simultaneously, the conversion of the FCAS data set here is dictated solely by the thermodynamic equilibrium parameters. Hence particle growth kinetics do not play an explicit role in this conversion analysis. Because all aerosols are assumed to have the same composition at equilibrium, the size of an individual aerosol is dependent primarily on the mass of H_2SO_4 contained in the aerosol, making the ternary and binary volumes proportional. The difference between the ternary and the FCAS binary total volumes, ΔV_{total}, is given by

$$\Delta V_{total} = \mathrm{Vol}_{STS} - \sum_i V_i^{FCAS} \quad (21)$$

where $\sum_i V_i^{FCAS}$ is the sum of volume over all size intervals i of the background distribution. The addition of STS volume in the ith interval ΔV_i of the FCAS distribution is defined here to be proportional to ΔV_{total}. Further, the proportionality constant is defined to be the fractional volume represented by the ith interval in the FCAS distribution as

$$\Delta V_i = (V_i^{FCAS} / \sum_i V_i^{FCAS}) \Delta V_{total} \quad (22)$$

The additional volume ΔV_i is distributed uniformly to the number of particles in the ith bin to predict the MASP distribution of size and volume in the PSC. As a result, the fractional change of average aerosol particle diameter (D_p), surface area (S), and volume (V) in the ith bin between the FCAS unmodified (binary) and the converted (ternary) distributions can be expressed as

$$\left(D_p^* / D_p\right)_i = \left(Vol_{STS} / \sum_i V_i^{FCAS} \right)^{1/3} \quad (23)$$

$$\left(S^* / S\right)_i = \left(Vol_{STS} / \sum_i V_i^{FCAS} \right)^{2/3} \quad (24)$$

$$\left(V^* / V\right)_i = \left(Vol_{STS} / \sum_i V_i^{FCAS} \right) \quad (25)$$

where the asterisk indicates the converted distribution parameters.

The comparison of the predicted and measured distributions is provided in Plate 2 for the second PSC peak corresponding temperatures between 189.7 and 191.2 K. Agreement is expected if STS is the actual composition of the observed PSC particles. The agreement between the modeled and the measured size distributions using both the APCM and the analytic expression (Plates 2d-2f and 2g-2i, respectively) provides strong support for STS composition. Both models give a reasonable reproduction of the number distribution of PSC aerosols represented by the MASP distribution, despite slight differences in the predictions of the two models. As discussed above, these model differences are considered indicative of the uncertainty in these calculations. The discrepancies between the model calculations and the MASP number distribution are clearly within the combined instrumental uncertainties. However, other uncertainties may contribute, such as the Kelvin effect for small aerosols, estimated to cause a difference of ~10% in the equilibrium composition. Alternatively, the PSC may contain either aerosols of a different composition or a mixture of compositions. Although modeling the growth of NAT or NAD is more difficult because a nucleation process is involved, a mixed-composition cloud is a possibility, as discussed by *Dye et al.* [1996] and as suggested by the impactor observations of *Goodman et al.* [1997].

NAT/NAD Formation from STS

The inference of STS aerosols for the conditions encountered by the ER-2 on July 28 has implications for the formation of crystalline NAT aerosols, either by crystallization on or from STS solutions. In laboratory studies of NAT formation the conditions necessary for crystallization are often referenced according to the corresponding saturation ratio S described in equation (4). Two calculations of the NAT saturation ratio in the gas phase as a function of T are shown in Figure 3a for the July 28 data set. For reference, the variation in Vol_{MASP} as a function of T also is shown (Figure 3b). For

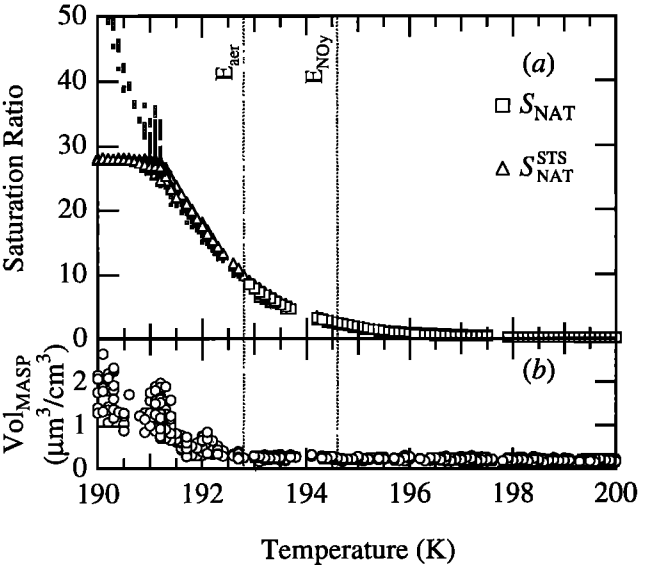

Figure 3. Saturation ratios of NAT as a function of T for the poleward leg of the flight track (UT < 86700 s). Plate 3a displays two apparent saturation ratios of NAT. The first, where $S = 0.9[NO_y^*]/[HNO_3]_{gas}^{NAT}$, is valid when no aerosols are formed (large open squares). (In regions of observed aerosol enhancement, values from this calculation are displayed as small open squares.) The second, where $S_{NAT}^{STS} = [HNO_3]_{gas}^{STS}/[HNO_3]_{gas}^{NAT}$, displays the saturation ratio of NAT when STS aerosol particles are inferred to be present (open triangles). Plate 3b displays MASP volume measurements for reference. The transition region defined by observed NO_y and aerosol enhancement is noted with vertical dashed lines.

regions without apparent aerosol enhancement (outside the PSC) the saturation ratio is calculated using $[HNO_3]_{total}$ as an estimate of $[HNO_3]_{gas}$ (equation (5), open squares). At temperatures below 192.8 K, where aerosol becomes enhanced and significant HNO_3 condensation can be inferred from observations, the apparent saturation ratio shown is no longer representative of the air parcel and is displayed in smaller symbols. Instead, S_{NAT} would be expected to fall to unity if the aerosols observed at temperatures below 192.8 K were composed of NAT at equilibrium.

In regions of enhanced aerosol a measure of $[HNO_3]_{gas}$ is required for calculations of S. While such measurements are not available for the flight of July 28, the previous analysis has shown that observations are consistent with STS composition. Having concluded that the bulk of aerosol encountered was composed of STS, we have used $[HNO_3]_{gas}^{STS}$ as a valid estimate of $[HNO_3]_{gas}$ for the air parcels encountered, even in regions where aerosol is enhanced. Thus the saturation ratio plotted as gray triangles is that of NAT in the presence of condensed STS aerosols (Figure 3a), where $[HNO_3]_{gas}^{STS}$ has been substituted for $[HNO_3]_{total}$ in the calculation of S.

The comparison of S_{NAT} and Vol_{MASP} in Figure 3 shows that significant increases in aerosol volume occur only at temperatures below 192.8 K, corresponding approximately to $S_{NAT} = 10$. In the presence of equilibrium STS, S_{NAT}^{STS} values are still ~10 at the point of significant aerosol growth. These

results are consistent with those found in Arctic PSC studies [*Dye et al.*, 1992; *Kawa et al.*, 1992] that, in part, led to the inclusion of a NAT nucleation barrier in some two-dimensional (2-D) model PSC parameterizations [*Considine et al.*, 1994]. However, in this analysis, as in analyses of the same Arctic PSC by *Carslaw et al.* [1994] and *Drdla et al.* [1994], this saturation ratio is shown to be merely coincidental, since the growth is assumed to be STS aerosol rather than NAT.

Crystallization of NAT and NAD from STS has been studied with mixed results. Both *Iraci et al.* [1995] and *Molina et al.* [1993] have observed nucleation of NAT from STS in thin-film studies and bulk freezing experiments, respectively. However, in other bulk freezing experiments, *Koop et al.* [1995] saw no nucleation of NAT from solutions of equilibrium STS composition until the ice frost point was reached. In aerosol studies, *Anthony et al.* [1997] did not observe crystallization of NAT from ternary aerosol droplets for temperatures from 190 to 204 K and observation times up to 3 hours. In the thin-film studies of *Iraci et al.* [1995], crystallization of NAT was observed within ~ 2 hours for $S_{NAT} \geq 14$. As shown in Figure 3, calculations of S^{STS}_{NAT} imply that NAT does not crystallize from STS solutions corresponding to $S_{NAT} \leq 28$. Although the aircraft observations could not follow an air parcel over a period of hours, temperature histories for the coldest air parcels indicate that they were below NAT temperatures for a period of 6-12 hours [*Kawa et al.*, 1997]. Thus the ASHOE/MAESA field observations are consistent with the *Koop et al.* [1995] and *Anthony et al.* [1997] results since there is no evidence, even at the lowest observed temperatures, that the gas phase was in equilibrium with the NAT phase. Had both condensed phases been in equilibrium with the gas phase, S^{STS}_{NAT} values should drop to 1. Therefore the importance of STS as a step in the mechanism for condensation of frozen NAT aerosols in the atmosphere remains uncertain. The equilibration of NAT in the atmosphere may require temperatures below the ice frost point or the presence of an impurity to induce NAT crystallization, as suggested by *Koop et al.* [1995].

Equilibrium Assumption

In the above analysis, aerosol particles are assumed to be in equilibrium with the gas phase. *Meilinger et al.* [1995] have developed a nonequilibrium aerosol growth model which indicates that NAT crystallization from STS may be possible in the nonequilibrium conditions of a strong cooling event. Temperature histories for the cloud encountered on July 28, 1994, indicate that sampled air masses experienced cooling of up to ~1.4 K per hour for about 18 hours prior to observation by the ER-2 [*Kawa et al.*, 1997]. This rate of cooling is relatively small compared to rates of more than 10 K per hour found in lee-wave events addressed by *Meilinger et al.* [1995]. Moreover, back trajectories indicate that air parcels sampled inside the PSC had traveled over ocean for at least 5 days prior to observation [*Kawa et al.*, 1997], precluding recent lee-wave cooling events. Therefore this nonequilibrium effect is not expected to influence the observations studied here. Rapid cooling rates associated with temperature fluctuations along air parcel trajectories [*Murphy and Gary*, 1995] may also create nonequilibrium conditions because of the sensitivity of the condensed phase to temperature (see Table 3). Although this effect cannot be evaluated here, the large number of samples in the PSC serve to average out the extreme departures from equilibrium.

The analysis here also assumes a single composition for the observed aerosol volume. The discrepancy between calculated values of $[HNO_3]^{STS}_{MASP}$ and $[HNO_3]^{STS}_{cond}$ could be explained by the added presence of NAT particles, as has been suggested by *Dye et al.* [1996]. If NAT particles were present, the observed aerosol volume associated with STS aerosol would necessarily be smaller, thereby improving the agreement in comparisons such as those in Figure 1. This possibility is supported by wire impactor results from the July 28 flight that indicate the presence of solid particles and even Type II PSC particles over limited regions of the flight track [*Goodman et al.*, 1997]. However, the solid particles accounted for only a small fraction of observed particles, and values of $S^{STS}_{NAT} > 1$ (Figure 3a) indicate that these particles were not NAT at equilibrium conditions. Thus most of the observed particles are assigned STS composition on the basis of comparisons of observations and models. *Dye et al.* [1996] reach the same conclusion based on the negative correlation of aerosol volume with temperature observed in this PSC encounter, indicative of a majority of liquid rather than solid crystalline aerosols.

Previous Arctic Results

Previous Arctic PSC observations made with instruments onboard the ER-2 have been evaluated for consistency with respect to NAT composition [*Dye et al.*, 1992; *Kawa et al.*, 1992]. Although NAT composition could not be ruled out in all sampling conditions, two important discrepancies were noted. First, large areas of NAT saturation were observed in several Arctic flights without an accompanying increase in aerosol volume. Second, $[HNO_3]_{FSSP}$ (equivalent to $[HNO_3]^{NAT}_{MASP}$ as used here) was greater than NO_y^* by a factor of 2 to 4 throughout most of the PSC encounter of January 24, 1989 [*Kawa et al.*, 1992]. Similar discrepancies with respect to NAT composition are evident in the current analysis. The current analysis reveals that a sharp increase in aerosol volume does not occur until S_{NAT} is ~10. In contrast, NO_y enhancement begins at somewhat lower values and correspondingly higher temperatures. In addition, at the lowest temperatures inside the cloud, $[HNO_3]^{NAT}_{MASP}$ is greater than $[HNO_3]_{total}$ (given by $0.9[NO_y^*]$) by up to 3 ppbv (Figure 1b). In the current analysis these discrepancies are not apparent in the STS composition results. While there are still some discrepancies between the values of $[HNO_3]^{STS}_{MASP}$ and $[HNO_3]^{STS}_{cond}$, $[HNO_3]^{STS}_{MASP}$ is generally a reasonable fraction (<1) of available HNO_3. Moreover, the ambient conditions of the flight of July 28, 1994, in the Antarctic appear to be comparable with those of the flight of January 24, 1989, in the Arctic, for which both *Carslaw et al.* [1994] and *Drdla et al.* [1994] also concluded that observations of a PSC are more consistent with STS composition. Therefore STS composition leads to more consistent results than NAT composition, both for the

Table 3. Average Sensitivity of the STS Calculation to Input Errors

Parameter Changed	Perturbation	$[HNO_3]^{STS}_{cond}$	$[HNO_3]^{STS}_{gas}$	$[wt\%_{HNO_3}]$	$[wt\%_{H_2SO_4}]$
H_2SO_4 mass	+35%	+22%	-1%	-4.0%	+9%
	+60%	+37%	-2%	-5.6%	+13%
T	+ 0.2%	-35%	+9%	-21%	+28%
	- 0.2%	+72%	-11%	+24%	-24%
P	+0.6%	+4%	-0.9%	+2%	-3%
	-0.6%	-4%	+0.8%	-2.2%	+3%
NO_y*	+15%	+43%	+9%	+17%	-17%
	-15%	-30%	-11%	-18%	+21%
H_2O	+ 1.00 ppmv	+220%	-24%	+48%	-42%
	- 1.00 ppmv	-58%	+18%	-38%	+70%
	- 2.00 ppmv	{no PSC}[a]	$\{\approx[HNO_3]_{total}\}$[a]	{<1%}[a]	{~ binary}[a]
	- 3.00 ppmv	{no PSC}	$\{\approx[HNO_3]_{total}\}$	{<1%}	{~ binary}

Average changes in the STS model output parameters (relative to values shown in Figures 1 and 2 and Plate 3) due to changes in the input parameters listed in the first column. For each input parameter, observed values for July 28 are perturbed by the values in the second column, with the resulting changes in derived quantities shown, respectively, in the remaining columns. The base value for H_2O is 5.0 ppmv.

[a]For values of $H_2O \leq 3.0$ ppmv the STS model predicts essentially binary H_2SO_4/H_2O aerosol with negligible amounts of condensed HNO_3, in direct conflict with observed NO_y enhancement.

Antarctic flight of July 28, 1994, and for some previous Arctic PSC flights.

Previous Antarctic Results

In the AAOE data set, the general character of the PSC observed on August 17, 1987 [*Fahey et al.*, 1989a], still strongly implies NAT composition. For the August 17 flight the sharp increase in aerosol volume corresponds very closely to the region of NAT saturation and displays the threshold behavior characteristic of a frozen hydrate. In addition, the comparison of condensed HNO_3 from aerosol measurements ($[HNO_3]_{aerosol}$, here $[HNO_3]_{MASP}$) with condensed HNO_3 from the NAT equilibrium model ($[HNO_3]_{net}$, here $[HNO_3]_{cond}$) agreed very closely in relative and absolute values. The ambient conditions under which the Antarctic PSC was observed during AAOE were significantly different than those of the ASHOE/MAESA observations. The growth of the AAOE PSC may have been forced by stronger cooling than the PSC of July 28, 1994, based on observations of mountain waves along the flight track [*Gary*, 1989]. Additionally, ice saturation and Type II PSC particles were noted within the PSC observed during AAOE [*Fahey et al.*, 1989a]. If the August 17 observations were to be reanalyzed in this study, similar results would be obtained because the calculation of $[HNO_3]^{NAT}_{gas}$ (equation (1)) is unchanged from 1987. Since $[HNO_3]_{gas}$ is lower for NAT than for STS, the AAOE results do not require or imply the presence of STS. In addition, the uncertainty in the background aerosol distribution arising from changes in the aerosol instrumentation complicates an analysis of the role of STS in this earlier data set.

The differences noted between the August 1987 and July 1994 Antarctic flights are consistent with a study by *Adriani et al.* [1995] in which lidar and particle counter observations over McMurdo Station, Antarctica, were compared. This study confirmed the existence of two distinct populations of Type I PSCs with distinct histories. Type Ia (nonspherical and probably crystalline) PSCs were associated with back trajectories that originated from high latitudes (>70°S) and had modest cooling rates of 1 to 5 K per day for 7 days prior to observation. These PSCs often were observed coexisting with Type II (ice) PSC particles. In contrast, air masses with Type Ib (spherical and probably liquid) PSCs had spent time at lower latitudes (60 to 70°S) in the 7 days prior to observation and had experienced cooling rates of 5 to 15 K per day. If the composition of Types Ia and Ib PSCs is assumed to be NAT and STS, respectively, these results suggest that both condensed phases are present over Antarctica. Other lidar observations of PSCs have shown that Type Ib aerosols appear frequently over both poles [*Toon et al.*, 1990; *Browell et al.*, 1990; *Rosen et al.*, 1993; *Stefanutti et al.*, 1995].

Carslaw et al. [1994] and *Tabazadeh and Toon* [1995] have suggested that STS PSCs may be most important in the Arctic, since frost-point temperatures occur less frequently. Sulfate aerosols may freeze at frost-point temperatures and are less likely to melt in the Antarctic since they would require temperatures of ~215 K. However, *Koop and Carslaw* [1996] indicate that frozen SAT aerosols may melt and form STS if temperatures are reduced below NAT formation temperatures and NAT formation fails to occur. Moreover, STS PSCs in the Antarctic may be most important in the edge region of the

Antarctic vortex and therefore will be significant in determining the areal extent and magnitude of ozone loss in the Antarctic. Thus, instead of eliminating the need for NAT composition in analyses, the good agreement found for STS composition in the Antarctic flight studied here reinforces the need to incorporate the ternary system in studies of polar ozone loss and to investigate further the separate conditions under which each type may form.

Implications

The availability of measured atmospheric parameters and the success of the STS composition model provide a unique basis with which to examine other issues related to Antarctic PSC formation. The uniqueness derives in part from the use of a comprehensive set of constituent and physical observations that are representative of atmospheric conditions. Issues of particular interest are differences between STS and NAT PSCs associated with heterogeneous reactivity and responses to perturbations from aircraft emissions. These differences have important implications for ozone loss processes in polar regions.

STS Reactivity

Because of the variable composition of STS aerosol and its continuous growth from background aerosol, the reactivity of STS surfaces is more difficult to characterize than that of solid surfaces. The wide range of conditions under which sulfate and STS aerosols can exist leads to corresponding large changes in the heterogeneous reactivity of those surfaces. Solid aerosols also display changes in reactivity as a function of ambient conditions, but those changes are relatively small over the limited range of conditions in which such phases may exist in the lower stratosphere. Although reaction probabilities on NAT surfaces vary with temperature and H_2O and HNO_3 partial pressures, the existence of NAT surfaces in an air parcel generally is sufficient for significant chlorine activation by the heterogeneous reactions

$$HCl + ClONO_2 \rightarrow Cl_2 + HNO_3 \qquad (R1)$$

and

$$H_2O + ClONO_2 \rightarrow HOCl + HNO_3. \qquad (R2)$$

[*Tolbert et al.*, 1987; *Abbatt and Molina*, 1992; *Kawa et al.*, 1997]. Thus the NAT saturation threshold often is used in models to define the high-reactivity region associated with PSCs [*Chipperfield et al.*, 1994]. In addition to a temperature dependence [*Zhang et al.*, 1995; *Hanson and Kavishankara*, 1994], the reactivity of STS particles also depends on $wt\%_{H_2SO_4}$, that corresponds to changes in a_{H_2O}. The reaction rates on STS or NAT PSCs also are a function of surface area that changes as the aerosols cool and grow.

In laboratory studies, *Zhang et al.* [1995] demonstrated that the rate of (R2) over the temperature range 215 to 195 K was independent of the HNO_3 concentration on liquid $H_2SO_4/H_2O/HNO_3$ surfaces. *Ravishankara and Hanson* [1996] have shown that the reactive uptake coefficients (γ) for (R1) and (R2) on liquid sulfate aerosols are larger than those on solids for temperatures between 195 K and the ice frost point. Liquid aerosol reactivities are less affected by high reactant concentrations because diffusion into the bulk liquid and away from the surface is faster. Solid particles under the same conditions can undergo alterations in surface properties because diffusion is slower. Also, *Ravishankara and Hanson* [1996] have found evidence that heterogeneous reactions on liquids are a combination of reactions in the bulk liquid and on the surface. While these studies were performed on liquid H_2SO_4/H_2O surfaces, *Ravishankara and Hanson* [1996] predict that $\gamma_{(R1)}$ may increase for STS particles with high HNO_3 concentrations due to the predicted larger solubility of HCl, while $\gamma_{(R2)}$ will remain comparable because H_2O concentrations remain similar. At low T, $\gamma_{(R2)}$ on liquid sulfate aerosols ranges from a factor of 10 to 200 larger than that on NAT surfaces; thus, far less surface area is required for liquid aerosols to process $ClONO_2$ as efficiently as NAT aerosols through (R2).

In applying reactivity studies to field observations, both the instantaneous conditions in an air parcel and the parcel's history are of value. *Kawa et al.* [1997] used a back-trajectory chlorine processing model to show that $\gamma_{(R1)}$ and $\gamma_{(R2)}$ for sulfate aerosol, when applied to calculated STS aerosol surface areas, are sufficient to account for the enhanced reactive chlorine observed on the flight of July 28. Here the instantaneous parameters are compared for NAT and STS at the observed ambient conditions. Making the same assumption that γ values for sulfate and STS aerosols are comparable, and using the formulation of *Hanson and Ravishankara* [1994], γ for heterogeneous loss of $ClONO_2$ on STS can be calculated along the flight track. The formulation used here describes the combined γ for both (R1) and (R2) and references the solubility of HCl to a_{H_2O}, that is equivalent to the relative humidity. Thus γ is primarily a function of a_{H_2O} and available HCl. By using a_{H_2O} as a reference, the specific composition of the aerosol is not needed for the calculation, provided condensed HNO_3 does not significantly change the solubilities and reaction rates. This assumption appears to be reasonable for the $ClONO_2$ reactions (D. R. Hanson, personal communication, 1996). The formulation of *Ravishankara and Hanson* [1996] also accounts for the dependence of γ on particle size through the competition of the diffusion and reaction rates according to the equation

$$\frac{1}{\gamma} = \frac{1}{\Gamma_{surf} + f(l/a)\Gamma_{calc}} + \frac{1}{\alpha} \qquad (26)$$

where Γ_{calc} is the uptake coefficient due to bulk reactions, Γ_{surf} is a surface reaction term, α is the mass accommodation coefficient that has values near unity, and $f(l/a)$ is a function that takes into account the spherical geometry and small size of stratospheric aerosol. An average reactive uptake coefficient γ_{eff} was then calculated as the number-density-weighted average of γ for all particle size bins in the MASP size distribution from 0.4 to 9.0 μm. For the conditions on July 28, using measured HCl along the flight track, γ_{eff} ranged from 0.01 to 0.54 in the temperature range 200 to 190 K, as shown in Plates 4a and 4e. Similar calculations were performed for fixed HCl fractions of total inorganic chlorine (HCl/Cl_y) of 0.9 and 0.1. For the observed conditions of July 28, γ_{eff} of 0.1 was reached

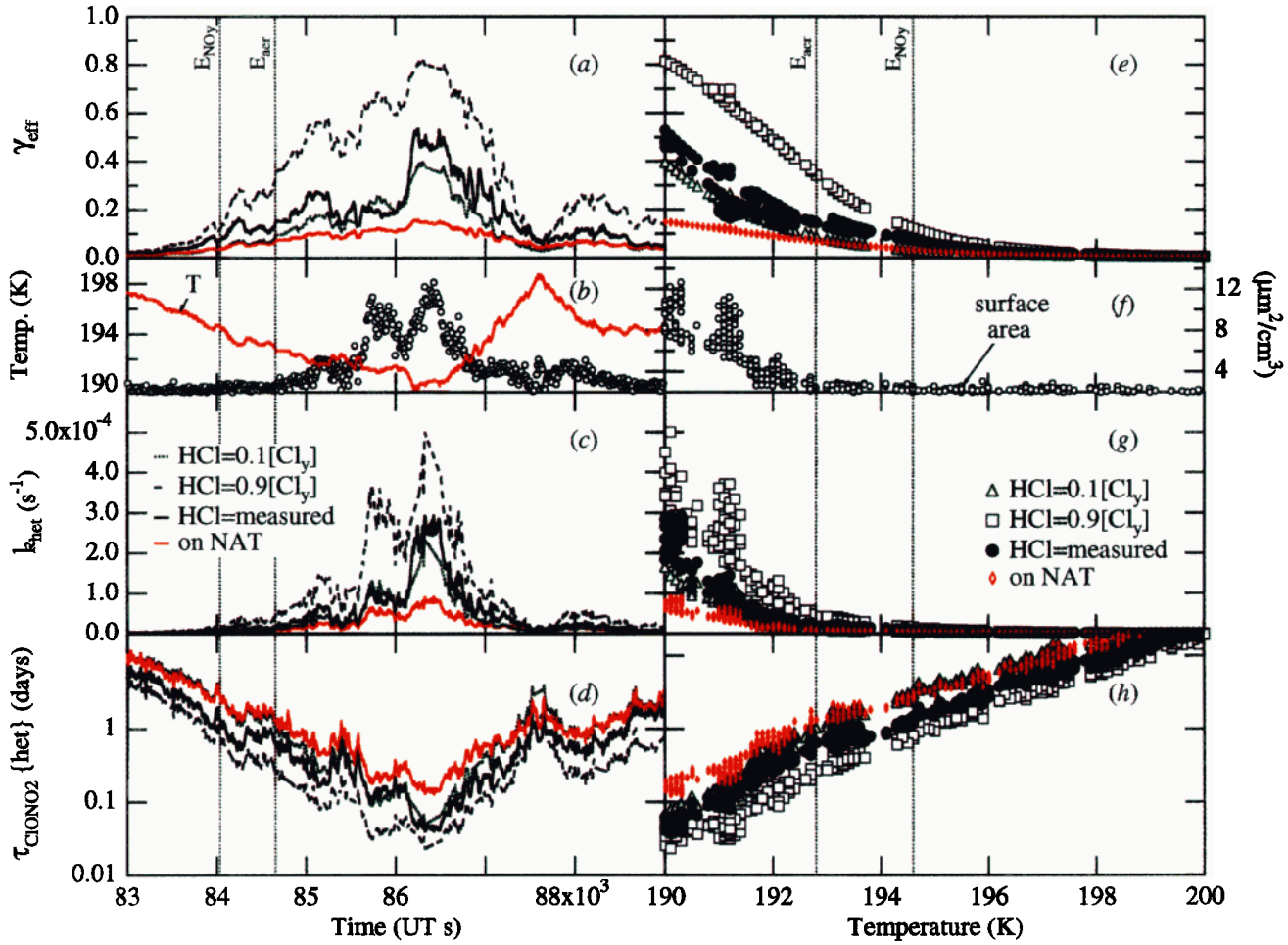

Plate 4. Heterogeneous reactivity of STS and NAT surfaces from observations for the July 28 flight. Panels on the left are displayed as a time series along the flight track, while panels on the right are displayed as a function of temperature for the poleward portion of the flight (UT < 86700 s). (a, e) Reactive uptake coefficient for $ClONO_2$ (γ_{eff}). (b, f) Temperature and observed aerosol surface area. (c, g) First-order rate coefficient for heterogeneous loss of $ClONO_2$ (k_{het}). (d, h) Time constant for heterogeneous loss of $ClONO_2$ (τ_{ClONO_2}). For STS, the quantities γ_{eff}, k_{het}, and τ_{ClONO_2} were calculated using HCl as observed during the July 28 flight (black solid line, solid circles), as well as for fixed HCl fractions of total inorganic chlorine (HCl/Cl_y) of 0.9 (blue solid line, open squares) and 0.1 (green dotted line, open triangles). For NAT, the same parameters for $ClONO_2$ loss using observed HCl are shown (red solid line, open diamonds). Vertical lines for NO_y enhancement (E_{NO_y}) and aerosol enhancement (E_{aer}) define the region of transition into the PSC on the poleward leg of the flight track. Data for a 0.1-Hz sample rate are shown, with the exception of temperature data that have a sample rate of 1 Hz.

in the transition region bounded by E_{NO_y} and E_{aer}. (The value $\gamma_{eff} = 0.1$ is used for comparison purposes as an average value often associated with chlorine processing on NAT surfaces.) Further inside the cloud, these values of γ_{eff} may change dramatically with small changes in ambient conditions due to a strong anticorrelation with T (Plate 4b) as well as sensitivity to available HCl and H_2O and the weighting of the aerosol size distribution. As described above, the assumption that HNO_3 does not alter the solubilities may be misleading at high concentrations of HNO_3, as found in the PSC where $wt\%_{HNO_3}$ reaches values of 40.

Using γ_{eff}, the pseudo-first-order rate constant for heterogeneous loss k_{het} can be calculated, along with the time constant for heterogeneous loss of $ClONO_2$, τ_{ClONO_2}, according to the equations

$$k_{het} = \gamma_{eff} \frac{<v>}{4} A \quad (27)$$

and

$$\tau_{ClONO_2} = \frac{1}{k_{het}}, \quad (28)$$

where A is the surface area density and <v> is the average velocity of a single $ClONO_2$ molecule at ambient T. These values apply only to the instantaneous conditions at the time of observation along the flight track, because depletion of the HCl reservoir as the reaction progresses leads to reduced values of γ_{eff} and k_{het} and increased values of τ_{ClONO_2}. Using $\tau_{ClONO_2} < 1$ day as the criterion for effective chlorine processing, the heterogeneous reactivity of the PSC becomes important in the transition region between E_{NO_y} and E_{aer} (Plates 4d, 4h), similar

to the analysis of γ_{eff}. However, at high values of HCl (HCl = 0.9 Cl_y), reactivity is enhanced in regions where neither NO_y nor aerosol enhancement were detected, and at low values of HCl (HCl = 0.1 Cl_y), $\tau_{ClONO_2} < 1$ day is only predicted for regions of observed aerosol enhancement. In Plate 4, the instantaneous values of γ, k_{het}, and τ_{ClONO_2} for $ClONO_2$ loss through (R1) on NAT particles are also shown, using observed HCl, observed aerosol surface area, and the formulation of *Hanson and Ravishankara* [1993]. Comparison of these quantities in Plate 4 reveals that STS composition leads to an increase in chlorine activation over that predicted for NAT particles by 30 to 300% across the entire PSC analysis region. Minimum values of τ_{ClONO_2} (~2 hours for STS and ~1 day for NAT) are also strikingly different. Thus, for the conditions observed during the July 28, 1994, flight, STS particles appear to be more effective than NAT at activating chlorine through (R1) and (R2).

Molina et al. [1993] and *Hanson et al.* [1994] have suggested that as temperatures approach the ice frost point, the chlorine activation efficiency of (R1) increases significantly for a range of compositions. For the flight of July 28, values of γ are up to a factor of 2 less for NAT than for STS at temperatures between 200 and 195 K (diamonds and solid circles, respectively, in Plate 4e); at temperatures below 195 K these values diverge further according to the formulations of *Hanson and Ravishankara* [1993, 1994]. Under conditions of comparable γ, the surface area present to facilitate chlorine activation becomes more important than other aerosol parameters. In Plate 4, observed surface area values are used for both STS and NAT calculations. However, in the results shown in Figures 1 and 2, the STS model predicts a lower total aerosol mass than the NAT model. The difference in surface area associated with a change in total mass depends on the particle size distribution. Therefore evaluating the efficiency of STS relative to NAT in facilitating chlorine activation requires a convolution of the higher reactive uptake coefficient for STS with a change in surface area that may or may not result from a lower aerosol mass. Despite this uncertainty, it is clear that, in general, NAT surface areas will have to be nearly four times larger than STS to be competitive.

Sensitivity of PSCs to Aircraft Emissions

The abundance and reactivity of PSCs will change in response to perturbations of the ambient mixing ratios of the component species. Increases in H_2O, HNO_3, or H_2SO_4 increase aerosol volume, although the response is different for STS than for either frozen hydrate. Important sources of such perturbations include emissions from the current subsonic aircraft fleet as well as those projected for a new fleet of HSCTs. Approximately 40% of the subsonic aircraft emissions occur in the stratosphere during the winter in the Northern Hemisphere [*WMO*, 1995], whereas nearly all HSCT emissions will occur in the stratosphere. The formation of PSCs is not included in the standard models used to evaluate the effects of HSCTs on climate and ozone in the current HSCT assessment [*Stolarski et al.*, 1995]. Thus our understanding of the potential role of PSCs in perturbations due to aircraft emissions is incomplete. The response of PSCs to aircraft emissions is difficult to include in 2-D assessment models because of uncertainties in our understanding of PSC formation processes and composition and because the zonal variability in formation conditions is not well represented. Generally, sensitivity tests are run in which the abundance of PSCs is parameterized using zonally averaged conditions in the model and various assumptions about the formation thresholds for NAT particles. For example, both *Pitari et al.* [1993] and *Considine et al.* [1994] allow for some supercooling prior to PSC formation. *Considine et al.* [1994] determine particle surface areas by allowing HNO_3 and H_2O to condense onto a lognormal distribution of aerosols. *Tie et al.* [1994] place the NAT formation threshold at temperatures higher than those required for thermodynamic equilibrium to account for errors both in model temperature at high latitudes and the impact of HNO_3 and H_2O emissions by HSCTs. PSC processes then are parameterized using time constants for heterogeneous reactions and removal of HNO_3 and H_2O through sedimentation of particles. However, only the PSC sensitivity tests of *Pitari et al.* [1993] included increases in aerosol surface area due to HSCT sulfur emissions and then only as a perturbation to the background aerosol size distribution on which NAT might grow. If NAT aerosols dominate the composition of PSCs during the polar winter, these parameterizations may adequately account for the apparent supersaturation of HNO_3 prior to crystallization. However, if STS is the dominant composition, PSCs will be extremely sensitive to changing levels of all three component species and therefore will respond to the perturbations caused by aircraft emissions very differently than NAT aerosols.

A useful estimate of the relative changes in the volume of NAT and STS PSCs resulting from aircraft emissions can be made by using the July 28 observations of NO_y, H_2SO_4, H_2O, P, and T as a basis. The changes in STS aerosol volume due to changes in constituent abundances can be examined with (20). Similar expressions can be made for NAT and NAD. At each point along the flight track, a new aerosol volume for each composition is obtained by using increased values of NO_y, H_2SO_4, and H_2O in calculating the terms on the right-hand side of (20). The increased values will be chosen to reflect the perturbations that would result from the emissions of an HSCT aircraft fleet. Because of the substitution of $[HNO_3]_{cond}$ for $[HNO_3]_{MASP}$ and the discrepancies between these two quantities shown in Figure 1, (20) will not provide the same absolute values of aerosol volume as that observed on July 28 for either NAT or STS. However, (20) will accurately reflect changes in aerosol volume due to perturbed ambient conditions. Although aerosol surface area is often more important than aerosol volume for estimating the reactivity in a PSC, surface area requires knowledge of the particle size distribution.

Increased values of NO_y and H_2O are based on Scenario IV of the HSCT assessment [*Stolarski et al.*, 1995], that assumes a fleet of 500 aircraft operating at Mach 2.4 at ~20 km altitude. The models predict perturbed levels of NO_y and H_2O based on predicted HSCT use and appropriate emission indices (EIs, expressed as grams per kilogram of fuel). In Scenario IV, EI_{NO_x} = 15 g/kg fuel and EI_{H_2O} = 1230 g/kg fuel, leading to increases of 20% and 7%, respectively, by the year 2015 for

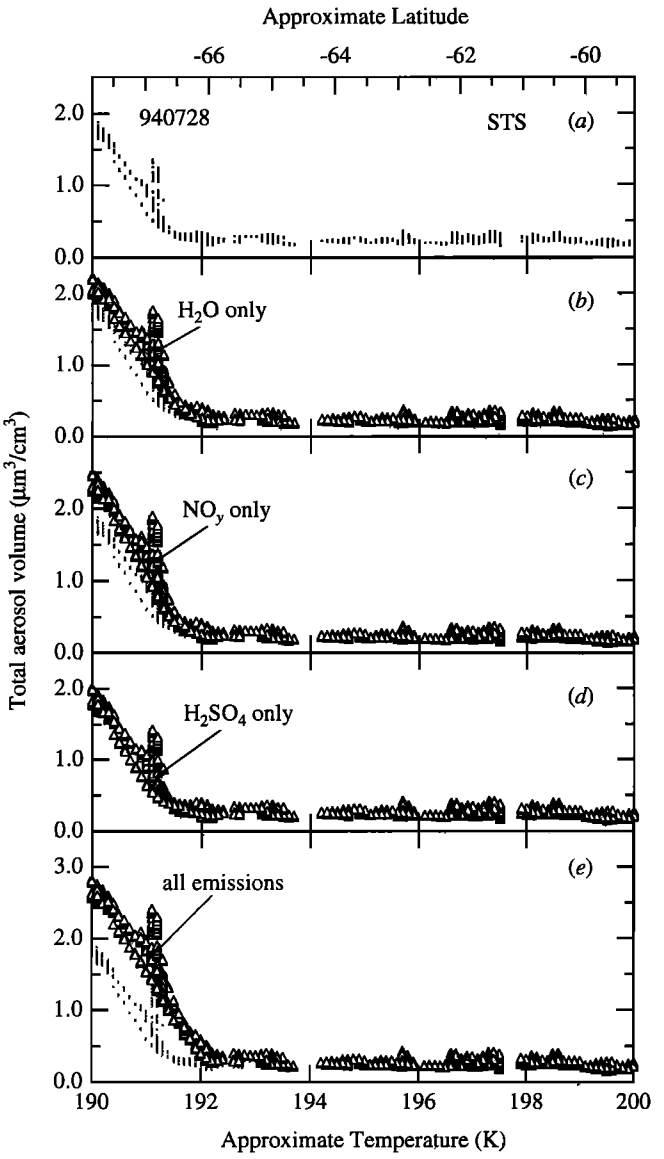

Figure 4. Total aerosol volume predicted by the STS model as a function of temperature and approximate latitude. Figure 4a displays the predicted aerosol volume for the July 28 flight; this trace is repeated in the other panels for reference. Other panels display the predicted aerosol volume for simulated perturbations in ambient H_2O (+7%) (b), NO_y (+20%) (c), H_2SO_4 (+15%) (d), and combined emissions (e) as a result of high-speed civil transport (HSCT) activity (Scenario IV, *Stolarski et al.* [1995]).

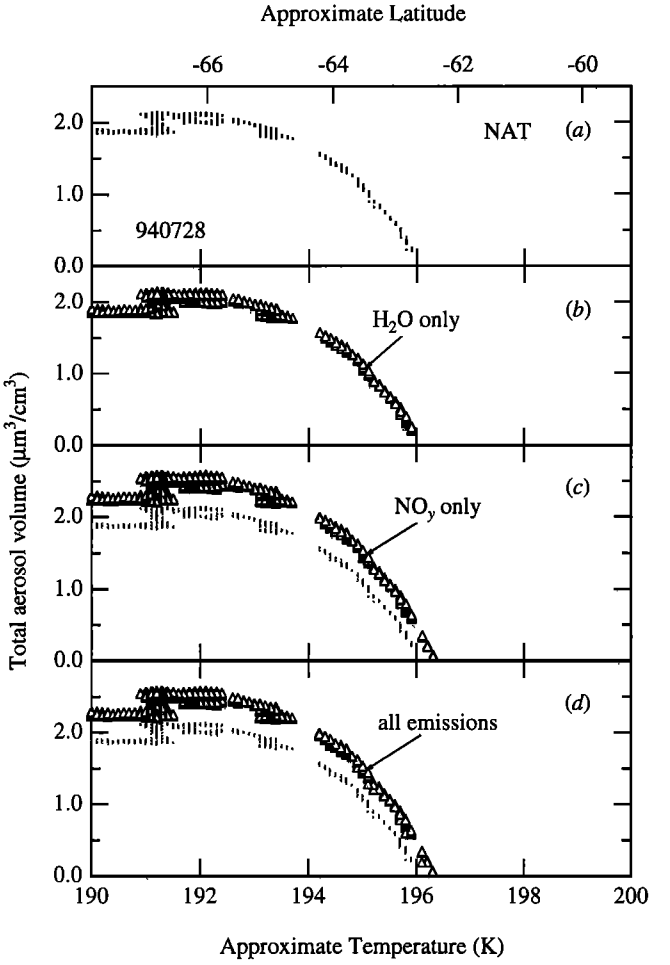

Figure 5. Total aerosol volume predicted by the NAT model as a function of temperature and approximate latitude. Figure 5a displays the predicted aerosol volume for the July 28 flight; this trace is repeated in the other panels for reference. Other panels display the predicted aerosol volume for simulated perturbations in ambient H_2O (+7%) (b), NO_y (+20%) (c), and combined emissions (d) as a result of HSCT activity (Scenario IV, *Stolarski et al.* [1995]).

60° to 70°S latitude and 18 to 20 km altitude (AER 2-D model) [*WMO*, 1995]. H_2SO_4 perturbations, that are primarily dependent on the amount of sulfur impurity contained in the fuel, also are affected by the rate of gas-to-particle conversion and the amount of preexisting sulfate aerosol through the resulting size distribution and associated fall velocities. *Weisenstein et al.* [1996] have shown that the perturbations to both surface area and H_2SO_4 mass increase with the fraction of sulfur emitted as particles in the aircraft plume. If the projected EI for sulfur (as SO_2) is 0.4 g/kg fuel, then the perturbation to total H_2SO_4 mass in a 2-D model at 60° to 70°S latitude and 18 to 20 km altitude would range from 7.5% when only a small fraction of sulfur is emitted as particles to 15% assuming 100% of sulfur is emitted as particles (D. Weisenstein, personal communication, 1996). For the purposes of this analysis, perturbations to total H_2SO_4 mass are assumed to be +15%. Since assessment models lack parameterizations of denitrification and dehydration that may reduce the calculated perturbations in H_2SO_4, H_2O, and NO_y, these calculations represent an upper limit to the expected perturbation in aerosol volume.

The calculations of perturbed aerosol volume were performed for both the STS and the NAT compositions, first by changing each component individually, then by combining the perturbations. The results for Vol_{STS} and Vol_{NAT} are shown in Figures 4 and 5, respectively, where values calculated for unperturbed conditions are shown in Figures 4a and 5a. These values are repeated in each subsequent panel as a reference. The change in Vol_{STS} due to a +7% perturbation in ambient H_2O, where all other conditions are fixed at observed

values, is approximately +40% with a range of 10 to 100% (Figure 4b). Although the influence of H_2O outside the cloud is less, a consistent 1% increase in total aerosol volume is found. The change in Vol_{STS} for NO_y is very similar to that noted for H_2O (Figure 4c), with an average increase of 45% (range of 15 to 110%) inside the cloud and the same consistent 1% increase to the background aerosol volume. The response to the H_2SO_4 perturbation (Figure 4d) is small relative to the other component species, but it has a different character than that seen for either H_2O or NO_y. For H_2SO_4 the average enhancement inside the PSC is +11%, while the background displays a 15% increase, comparable to the change in H_2SO_4 abundance.

The combined effect of the NO_y, H_2O, and H_2SO_4 perturbations is shown in Figure 4e, where larger increases in total aerosol volume are evident. The average increase in Vol_{STS} inside the PSC is 93%, with values ranging from 54% at temperatures near 190 K to 260% at temperatures near 192 K. The increases in Vol_{STS} are largest in the transition region between background and PSC aerosol due to the different temperature dependences of the H_2O and HNO_3 perturbations relative to that of H_2SO_4. Because of its low vapor pressure, nearly all H_2SO_4 added to an air parcel is added to the condensed phase at stratospheric temperatures. Thus the response of Vol_{STS} to perturbations in H_2SO_4 is effectively independent of temperature and appears as a constant offset to the initial values of Vol_{STS}. In contrast, the uptake of H_2O and HNO_3 by aerosols is strongly temperature dependent. The fractional response of Vol_{STS} to a change in the gas-phase abundance of H_2O or HNO_3 decreases with decreasing temperature. Therefore the maximum fractional change in Vol_{STS} occurs at temperatures ~192 K where the offset due to H_2SO_4 is a significant fraction of the unperturbed aerosol and where the fractional increase due to H_2O and HNO_3 is large. An important feature in Figure 4e is that the increase in the temperature range of enhanced aerosol volume corresponds to an increased areal extent in polar regions. For the same temperature distribution along the July 28 flight track, significant increases in STS aerosol volume over background would appear in regions ~0.7 K higher in temperature and ~90 km further equatorward.

As expected, the response to perturbations is different for NAT. In Figure 5b, no significant increases in Vol_{NAT} are apparent as a result of perturbations to H_2O. Increased H_2SO_4 has no impact on the NAT equilibrium expression, leaving Vol_{NAT} insensitive to such changes. Only the perturbation to NO_y (HNO_3) causes an increase inside the cloud with average values of 27% (range of 20 to 50%). The increase in Vol_{NAT} due to the combined emissions is not significantly higher, averaging 27.2% inside the cloud. The effect of the combined perturbations to H_2O and NO_y on NAT formation would extend the PSC of July 28 to regions ~0.3 K higher in temperature and 7 km further equatorward, much less than found for STS. Although H_2SO_4 increases have no impact on the calculation of Vol_{NAT}, such changes might alter the size and number density of sulfate nuclei, and hence the surface area and denitrification potential of NAT PSCs and the probability of NAT formation.

In previous studies of PSC formation probability, *Peter et al.* [1991] found that the increase in NO_y and H_2O due to emissions of 600 stratospheric aircraft more than doubled the probability of NAT PSC formation in Northern Hemisphere winter. More recently, *Pawson et al.* [1995] used a 29-year daily temperature record to estimate the PSC formation potential in the Northern Hemisphere. This study found that for criteria of $T < 195$ K and $P = 50$ hPa, PSCs form 50% of the time over an area enclosing up to 2.5% of the Northern Hemisphere poleward of 40°N. Perturbations to ambient NO_y, H_2O, and H_2SO_4 in the Southern Hemisphere may be expected to raise the temperature for STS PSC formation by 0.7 K, thereby significantly increasing the estimated area in which any PSC formation occurs. Alternatively, the effect of aircraft emissions may be seen as leading to an increased potential for PSC formation at a given temperature. In the Northern Hemisphere, the EI_{NO_x}, EI_{H_2O}, and EI_{SO_2} values in Scenario IV lead to perturbations of +40-60% in NO_y, +10-20% in H_2O, and +40-50% in H_2SO_4 at 60 to 70°N latitude and 18 to 20 km altitude due to the proximity of the proposed flight corridors [*Stolarski et al.*, 1995; D. Weisenstein, personal communication, 1996]. Thus the effect of projected aircraft emissions on PSCs in the Arctic may be even larger than that shown above for the observed Antarctic PSC, especially in light of studies by *Carslaw et al.* [1994] and *Tabazadeh and Toon* [1995] that suggested STS PSCs may be more prevalent in the Arctic. In studies by *Pitari et al.* [1993] and *Considine et al.* [1994], adding a NAT PSC parameterization to the 2-D model reduced the sensitivity of ozone to HSCT emissions due to the enhanced NO_y removal rate and reduced residence time of emitted NO_x. However, the exception was the Antarctic spring when the larger surface area of NAT particles led to a longer PSC season and increased local ozone loss. On the basis of the above comparison of STS and NAT aerosols, the effect of increased surface area and reactivity in polar regions as noted by *Pitari et al.* [1993] and *Considine et al.* [1994] may be enhanced in the case of STS PSCs and could have important implications for ozone loss in the Arctic spring.

Conclusions

Antarctic NO_y and aerosol measurements made in PSCs during ASHOE/MAESA have been analyzed in a manner similar to previous Antarctic (AAOE) and Arctic (AASE) PSC studies. In addressing the composition of PSC cloud particles and the apparent interhemispheric differences noted in previous studies, some important similarities and differences were revealed. The composition of the observed Type I PSC aerosols was evaluated using equilibrium expressions for the frozen hydrates NAT and NAD and the liquid STS. The equilibrium abundance of condensed HNO_3 was calculated for each phase and compared to estimates made using observations of aerosol volume and NO_y. The specific criteria used to compare these three derived quantities were predictions of the onset and abundance of HNO_3 in the PSC aerosol as observed along the flight track or as a function of temperature.

As in previous polar data sets from AAOE and AASE, the ASHOE/MAESA results confirm the existence of Type I PSCs

that form at temperatures higher than the ice frost point, and all three data sets confirm the presence of significant amounts of NO_y in observed PSC particles. The test of NAT composition in this analysis reveals large regions along the flight track in which conditions are supersaturated with respect to NAT without a corresponding increase in aerosol volume, as seen in previous Arctic studies. This observation in the Antarctic reinforces the likelihood that a nucleation barrier to NAT crystallization can play a role in PSC formation. NO_y redistribution could explain some of the discrepancies found in tests of NAT composition inside a PSC but cannot explain the large regions of observed supersaturation where no PSC aerosol is observed. Also, while tests of NAD composition indicate better agreement than NAT with respect to the onset criterion, much larger amounts of redistributed NO_y would be required for complete agreement. The STS composition model accurately represents the continuous growth from background aerosol and provides the best quantitative and qualitative agreement in comparisons using measurements of NO_y and aerosol. In addition, STS size distributions modeled as the addition of STS HNO_3 and H_2O to the FCAS distribution are in good agreement with observed PSC size distributions for temperatures less than 191 K, although discrepancies and uncertainties are apparent. Despite some differences in the equilibrium models of *Carslaw et al.* [1995a, b] and *Tabazadeh et al.* [1994b], both STS models provide better agreement with observations than either of the frozen hydrates. The results of the current analysis for the Antarctic supports the conclusion drawn by *Carslaw et al.* [1994] and *Drdla et al.* [1994] that in the Arctic some PSCs are likely composed of STS.

This evidence of STS PSC aerosols in the Antarctic has strong implications for our understanding of the evolution of PSCs during the polar winter as well as our ability to model PSC processes. STS composition implies a different PSC formation mechanism than the threshold behavior associated with NAT formation. Instead, STS aerosols form in a continuous uptake process from background sulfate aerosols as temperature is decreased. If the observed aerosols are assumed to be STS in equilibrium, enough HNO_3 remains in the gas phase that calculated NAT saturation ratios are as high as 28. This suggests that the formation of NAT aerosols does not require maximum ratios of 10 as previously suggested. NAT crystallization may require some other nucleation mechanism, whether it be reaching the ice frost point followed by warming, or through some nonequilibrium uptake as suggested by *Meilinger et al.* [1995].

The presence of liquid rather than solid-crystalline NAT or NAD aerosols affects the calculated rates of heterogeneous reactions in sampled air parcels. Values of γ for STS are 30 to 300% greater than those for NAT at temperatures less than 195 K and for the entire PSC analysis region. The $ClONO_2$ lifetime with respect to heterogeneous loss for STS aerosol was found to reach one day or less in the transition region between observed NO_y and MASP aerosol enhancement and to be highly sensitive to T, H_2O, HCl, and surface area.

Compared to NAT, STS aerosol volume displayed a greater response to perturbations in H_2O, HNO_3, and H_2SO_4 from predicted HSCT emissions. The combined effect of the perturbations given in the current assessment is a PSC containing 50 to 260% more STS aerosol volume and extending to regions 0.7 K higher in temperature than the PSC observed on July 28. The presence of STS aerosols in the polar stratosphere reinforces the need to expand the treatment of PSCs in studies of polar ozone loss, both for the understanding of the current state of the stratosphere and for the predictions of the impact of HSCTs.

Appendix: Experimental Uncertainties

The significance of the agreement between observations and models must be judged in light of the uncertainties in both the measured and the derived quantities involved in the analysis. The single largest source of error in this analysis is the lack of direct measurements of H_2O. The error in our estimate of available water is difficult to characterize, but sensitivity tests were carried out by running the complete analysis at five integer values of H_2O from 2.0 to 6.0 ppmv. The results of these tests are described in more detail below. In the absence of direct measurements and a reasonable estimate of the error, the uncertainty in the derived quantities below was determined independently of the influence of H_2O.

Aerosol

The MASP instrument is a modification of the Forward Scattering Spectrometer Probe (FSSP) used in previous aircraft field studies. This new instrument is described by *Baumgardner et al.* [1996], while the FSSP used during AASE is described in *Baumgardner et al.* [1992]. The minimum size from MASP used in this analysis was 0.30 μm in diameter; the minimum detectable size from the FSSP used in Arctic analyses [*Kawa et al.*, 1992; *Dye et al.*, 1992] was 0.37 μm. Thus the total volumes calculated for the Arctic data and the new Antarctic data should be comparable; in fact, aerosols smaller than 0.37 μm made no contribution to the total volume in the Antarctic PSC. The FSSP used in AAOE had a minimum detectable size of 0.8 μm [*Baumgardner et al.*, 1989]. In previous Antarctic analyses the total volume in sizes less than 0.8 μm was assumed to be negligible in PSC events. The current analysis shows that on average, 10 to 20% (20 to 30%) of total aerosol volume is associated with particle sizes between 0.3 and 0.8 μm in diameter inside (outside) the cloud. Even if 10 to 20% of the aerosol volume was missed in the PSC encountered during AAOE, this relatively small change would not significantly affect the conclusions reached in that analysis [*Fahey et al.*, 1989a]. Therefore the analysis of PSC observations made here is consistent with previous studies.

The propagated uncertainty of MASP has not yet been fully analyzed (D. Baumgardner, personal communication). For the purposes of this analysis, estimated uncertainties in particle volume, number concentration, and sizing are ~60%, 25%, and 14%, respectively. The uncertainty in $[HNO_3]^{NAT}_{MASP}$ is approximately the same as that in particle volume, since the

relative errors of P and T are negligible; for $[HNO_3]^{NAD}_{MASP}$ and $[HNO_3]^{STS}_{MASP}$ the uncertainty is larger due to the uncertainty in particle density (±65% and ±75%, respectively). An additional uncertainty in the MASP measurements is the refractive index chosen for interpretation of the raw data. Refractive indices for amorphous, α-, and β-NAT reported by *Middlebrook et al.* [1994] range from 1.43 to 1.51 at temperatures between 140 and 185 K, and the refractive index for amorphous NAD is 1.44 at 140 K. Therefore a refractive index of 1.44 was used to interpret all aerosol data for the NAT and NAD analyses. STS, which is assumed to have a lower refractive index at cold temperatures due to its high water content, was analyzed at a refractive index of 1.40. This value is slightly lower than the average refractive index predicted by *Steele and Hamill* [1981] for binary H_2SO_4 solutions inside the PSC. While the temperature dependence of the relevant refractive index introduces some error into the calculations, it is not expected to significantly change the results. Furthermore, the difference in total aerosol volume between data analyzed at 1.40 and 1.44 is ~30%. Therefore errors of ±0.4 in refractive index are expected to fall within this uncertainty.

The uncertainties of the FCAS instrument, which measures particles with diameters ranging from 0.06 to 3.00 μm, have not been fully evaluated. Thus the error in H_2SO_4 mass derived from FCAS is unknown. However, uncertainties are assumed to be of the order of those estimated above for MASP measurements. In the region of overlapping sizes measured by FCAS and MASP in the background aerosol, differences in total volume (MASP minus FCAS) average 35%, with some values as high as 60%. Because these errors all fall within the uncertainty of the two instruments, values of H_2SO_4 mass derived from FCAS may be treated as consistent with the aerosol volumes measured by MASP. The value of H_2SO_4 mass derived from FCAS measurements is shown in Plate 1c. Although *Dye et al.* [1996] have chosen to increase H_2SO_4 mass derived from FCAS by the average 35% difference, this change does not significantly alter the results or the conclusions drawn. For the sake of comparison the value of H_2SO_4 mass used by *Dye et al.* [1996] is used in the sensitivity test of the STS model results (Table 3), as is the 60% increase over FCAS values corresponding to the largest differences between the two instruments.

$[HNO_3]_{gas}$

The error in $[HNO_3]_{gas}$ is dependent on the error in the laboratory measurements of saturation conditions combined with the errors in the input measurement variables. The uncertainties associated with measured P and T are ±0.6% and ±0.2%, respectively [*Chan et al.*, 1989]. The error in H_2O is neglected in this analysis. Thus for NAT, with an error in the laboratory measurements of ±30%, the uncertainty in $[HNO_3]^{NAT}_{gas}$ is ±40%. For NAD, the ±65% uncertainty in laboratory measurements, combined with the error in T and P, gives an uncertainty of ±72%. No error analysis is available for the STS equilibrium models. Therefore the error in $[HNO_3]^{STS}_{gas}$ is unknown but is assumed in this analysis to be within a factor of two.

NO_y, NO_y^*, $[HNO_3]_{cond}$, $[NO_y]_{aer}$

The NO_y measurement is accurate to about ±15%. There is some uncertainty in the maximum size of particles that reach the inlet that could affect quantities derived from NO_y, especially A_{eff} and therefore $[NO_y]_{aer}$. However, the inertial cutoff of the inlet housing is known to be ~4 μm, and for this flight there is no evidence in the MASP measurements of particles larger than 4 μm. Therefore the effect of this uncertainty should be negligible. The error in NO_y^* as an estimate of total NO_y in regions unperturbed by PSCs is about ±15% as derived from the combination of the standard deviation in the NO_y/N_2O relationship, the ±2% uncertainty in ATLAS N_2O measurements, and the ±15% uncertainty in NO_y measurements. The error in $[HNO_3]_{cond}$ is a combination of the error in $[HNO_3]_{gas}$ with the error in the estimated HNO_3 fraction of NO_y for NAT and NAD. For STS the error in $[HNO_3]_{cond}$ is the error of calculated condensed HNO_3 in the model itself. Thus the error estimates are 43% for NAT, 73% for NAD, and a factor of 2 for STS. A 14% sizing uncertainty in the MASP instrument combined with the nominal accuracy of ±30% in the calculation of A results in an uncertainty of ±35% in the calculation of A_{eff} for measurements at cruise altitude. However, since the behavior of particles in the NO_y inlet is difficult to characterize precisely, the errors in A_{eff} may be larger than estimated, especially in the case of NAT and NAD due to the assumption of spherical particles. This results in a lower limit to the propagated uncertainty in $[NO_y]_{aer}$ of approximately 36% for NAT, 45% for NAD, and 52% for STS.

STS Composition

Errors in the APCM ternary solution model that result from errors in laboratory measurements and temperature extrapolations have not been explicitly determined. Instead, for the purposes of this analysis, sensitivity tests were performed using the stated error limits of the relevant input values. The ternary solution model is extremely sensitive to a number of variables, including available H_2SO_4 mass, NO_y^*, T, and P. The average changes in $wt\%_{HNO_3}$, $wt\%_{H_2SO_4}$, $[HNO_3]^{STS}_{cond}$, and $[HNO_3]^{STS}_{gas}$ calculated by the APCM due to individual input errors are given in Table 3.

Differences between the analytic expression and the comprehensive model of *Carslaw et al.* [1995a, b] are 7 to 10% for $[HNO_3]^{STS}_{cond}$ and $[HNO_3]^{STS}_{gas}$. As with the APCM, the error in the comprehensive model has not been determined. A factor of 2 was used as an estimate of the error (due to the combined errors from laboratory measurements and temperature extrapolations) in $[HNO_3]^{STS}_{cond}$ from both models for comparison to the NAT- and NAD-derived quantities. Most of the discrepancies between the analytic expression and the APCM also fall within this uncertainty envelope.

H_2O Sensitivity

Separate calculations of $[HNO_3]_{cond}$, $[HNO_3]_{MASP}$, and $[NO_y]_{aer}$ were performed for all three compositions at five different H_2O mixing ratios. The figures shown here are the results of the calculation using an H_2O mixing ratio of 5.0

ppmv; values of 2.0, 3.0, 4.0 and 6.0 ppmv also were used in separate analyses to encompass a reasonable range of possible values, including the possibility of dehydration in the polar vortex. The changes to the results of the STS calculation at the upper and lower H_2O limits are noted in Table 3. The NAT and NAD models are also sensitive to changes in ambient H_2O in $[HNO_3]_{cond}$. ($[HNO_3]_{MASP}$ and $[NO_y]_{aer}$ for NAT and NAD are insensitive to changes in ambient H_2O due to the fixed density and $wt\%_{HNO_3}$ in the frozen hydrates.) Regions of supersaturation for NAT can be eliminated at values of H_2O = 2.0 ppmv, but this leads to large discrepancies in the abundance of HNO_3 inside the PSC ($[HNO_3]^{NAT}_{cond} < [HNO_3]^{NAT}_{MASP}$ by ~70%, $[NO_y]^{NAT}_{aer} < [HNO_3]^{NAT}_{cond}$ by 30%). Similarly, regions of supersaturation can be eliminated for NAD at values of H_2O = 3.0 ppmv but with accompanying discrepancies ($[HNO_3]^{NAD}_{cond} < [HNO_3]^{NAD}_{MASP}$ by ~80%, $[NO_y]^{NAD}_{aer} < [HNO_3]^{NAD}_{cond}$ by 40%). However, the sensitivity to H_2O does not change the general character of agreement for either model relative to that displayed in Figures 1 and 2 for a H_2O mixing ratio of 5.0 ppmv.

Acknowledgments. The authors wish to thank L. T. Iraci, S. R. Kawa, K. S. Carslaw, and D. R. Hanson for help and discussions; K. A. Wolfe for editorial assistance; and NASA's Upper Atmosphere Research, Atmospheric Chemistry Modeling and Analysis, and High-Speed Research Programs for supporting this effort.

References

Abbatt, J. P. D., and M. J. Molina, Heterogeneous interactions of $ClONO_2$ and HCl on nitric acid trihydrate at 202 K, *J. Phys. Chem.*, *96*, 7674-7679, 1992.

Adriani, A., T. Deshler, G. Di Donfrancesco, and G P. Gobbi, Polar stratospheric clouds and volcanic aerosol during spring 1992 over McMurdo Station, Antarctica. Lidar and particle counter comparisons, *J. Geophys. Res.*, *100*, 25,877-25,897, 1995.

Anthony, S. E., T. B. Onasch, R. T. Tisdale, R. S. Disselkamp, M. A. Tolbert, and J. C. Wilson, Laboratory studies of ternary $H_2SO_4/HNO_3/H_2O$ particles: Implications for polar stratospheric cloud formation, *J. Geophys. Res.*, in press, 1997.

Arnold, F., Stratospheric aerosol increases and ozone destruction: Implications from mass spectrometer measurements, *Ber. Bunsenges. Phys. Chem.*, *96*, 339-350, 1992.

Baumgardner, D., J. E. Dye, and B. W. Gandrud, Calibration of the Forward Scattering Spectrometer Probe used on the ER-2 during the Airborne Antarctic Ozone Experiment, *J. Geophys. Res.*, *94*, 16,475-16,480, 1989.

Baumgardner, D., J. E. Dye, R. G. Knollenberg, and B. W. Gandrud, Interpretation of measurements made by the Forward Scattering Spectrometer Probe (FSSP-300) during the Airborne Arctic Stratospheric Expedition, *J. Geophys. Res.*, *94*, 8035-8046, 1992.

Baumgardner, D., J. E. Dye, B. Gandrud, K. Barr, K. Kelly, and K. R. Chan, Refractive Indices of aerosols in the upper troposphere and lower stratosphere, *Geophys. Res. Lett.*, *23*, 749-752, 1996.

Berland, B. S., D. R. Haynes, K. L. Foster, M. A. Tolbert, S. M. George, and O. B. Toon, Refractive indices of amorphous and crystalline HNO_3/H_2O films representative of polar stratospheric clouds, *J. Phys. Chem.*, *98*, 4358-4364, 1994.

Browell, E. V., C. F. Butler, S. Ismail, P. A. Robinette, A. F. Carter, N. S. Higdon, O. B. Toon, M. R. Schoeberl, and A. F. Tuck, Airborne lidar observations in the wintertime Arctic stratosphere: Polar stratospheric clouds, *Geophys. Res. Lett.*, *17*, 385-388, 1990.

Carslaw, K. S., B. P. Luo, S. L. Clegg, T. Peter, P. Brimblecombe, and P. J. Crutzen, Stratospheric aerosol growth and HNO_3 gas phase depletion from coupled HNO_3 and water uptake by liquid particles, *Geophys. Res. Lett.*, *21*, 2479-2482, 1994.

Carslaw, K. S., S. L. Clegg, and P. Brimblecombe, A thermodynamic model of the system HCl- HNO_3-H_2SO_4-H_2O, including solubilities of HBr from <200 to 328 K, *J. Phys. Chem.*, *99*, 11,557-11,574, 1995a.

Carslaw, K. S., B. Luo, and T. Peter, An analytic expression for the composition of aqueous HNO_3- H_2SO_4 stratospheric aerosols including gas phase removal of HNO_3, *Geophys. Res. Lett.*, *22*, 1877-1880, 1995b.

Chan, K. R., S. G. Scott, T. P. Bui, S. W. Bowen, and J. Day, Temperature and horizontal wind measurements on the ER-2 aircraft during the 1987 Airborne Antarctic Ozone Experiment, *J. Geophys. Res.*, *94*, 11,573-11,587, 1989.

Chipperfield, M. P., D. Cariolle, and P. Simon, A 3D transport model study of chlorine activation during EASOE, *Geophys. Res. Lett.*, *21*, 1467-1470, 1994.

Considine, D. B., A. R. Douglass, and C. H. Jackman, Effects of a polar stratospheric cloud parameterization on ozone depletion due to stratospheric aircraft in a two-dimensional model, *J. Geophys. Res.*, 99, 18,879-18,894, 1994.

Crutzen, P. J., and F. Arnold, Nitric acid cloud formation in the cold Antarctic stratosphere: A major cause for the springtime "ozone hole," *Nature*, *324*, 651-655, 1986.

Delaplane, R. G, I. Taesler, and I. Olovsson, Hydrogen bond studies. XCIII. Oxonium ion in nitric acid monohydrate, *Acta Crysallogrt., Ser. B31*, 1486-1489, 1975.

Disselkamp, R. S., S. E. Anthony, A. J. Prenni, T. B. Onasch, and M. A. Tolbert, Crystallization kinetics of nitric acid dihydrate aerosols, *J. Phys. Chem.*, *100*, 9127-9137, 1996.

Drdla, K., A. Tabazadeh, R. P. Turco, M. Z. Jacobsen, J. E. Dye, C. Twohy, and D. Baumgardner, Analysis of the physical state of one Arctic polar stratospheric cloud based on observations, *Geophys. Res. Lett.*, *21*, 2475-2478, 1994.

Dye, J. E., D. Baumgardner, B. W. Gandrud, S. R. Kawa, K. K. Kelly, M. Loewenstein, G. V. Ferry, K. R. Chan, and B. L. Gary, Particle size distributions in Arctic polar stratospheric clouds, growth and freezing of sulfuric acid droplets and implications for cloud formation, *J. Geophys. Res.*, *97*, 8015-8034, 1992.

Dye, J. E., et al., In-situ observations of an Antarctic polar stratospheric cloud during ASHOE/MAESA: Similarities with Arctic observations, *Geophys. Res. Lett.*, 23, 1913-1916, 1996.

Fahey, D. W., K. K. Kelly, G. V. Ferry, L. R. Poole, J. C. Wilson, D. M. Murphy, M. Loewenstein, and K R. Chan, In situ measurements of total reactive nitrogen, total water, and aerosol in a polar stratospheric cloud in the Antarctic, *J. Geophys. Res.*, *94*, 11,299-11,315, 1989a.

Fahey, D. W., D. M. Murphy, K. K. Kelly, M. K. W. Ko, M. H. Proffitt, C. S. Eubank, G. V. Ferry, M. Loewenstein, and K. R. Chan, Measurements of nitric oxide and total reactive nitrogen in the Antarctic stratosphere: Observations and chemical implications, *J. Geophys. Res.*, *94*, 16,665-16,681, 1989b.

Fahey D. W., K. K. Kelly, S. R. Kawa, A. F. Tuck, M. Loewenstein, K. R. Chan, and L. E Heidt, Observation of denitrification and dehydration in the winter polar stratospheres, *Nature*, *344*, 321-324, 1990.

Fox, L. E., D. R. Worsnop, M. S. Zahniser, and S. C. Wofsy, Metastable phases in polar stratospheric aerosols, *Science*, *267*, 351-355, 1995.

Gao, R. S., et al., Partitioning of the reactive nitrogen reservoir in the lower stratosphere of the Southern Hemisphere: Observations and modeling, *J. Geophys. Res.*, *102*, 3935-3949, 1997.

Gary, B. L., Observational results using the Microwave Temperature Profiler during the Airborne Antarctic Ozone Experiment, *J. Geophys. Res.*, *94*, 11,223-11,231, 1989.

Goodman J., S. Verma, R. F. Pueschel, P. Hamill, G. V. Ferry, and D. Webster, New evidence of size and composition of polar stratospheric cloud particles, *Geophys. Res. Lett.*, 24, 615-618, 1997.

Hamill, P. R , R. P. Turco, and O. B. Toon, On the growth of nitric and sulfuric acid aerosol particles under stratospheric conditions, *J. Atmos. Chem.*, *7*, 287-315, 1988.

Hanson, D. R., The uptake of HNO_3 onto ice, NAT, and frozen sulfuric acid, *Geophys. Res. Lett.*, *19*, 2063-2066, 1992.

Hanson, D., and K. Mauersberger, Laboratory studies of the nitric acid trihydrate: Implications for the south polar stratosphere, *Geophys. Res. Lett.*, *15*, 855-858, 1988.

Hanson, D. R., and A. R. Ravishankara, Reaction of $ClONO_2$ with HCl on NAT, NAD, and frozen sulfuric acid and hydrolysis of N_2O_5 and $ClONO_2$ on frozen sulfuric acid, *J. Geophys. Res.*, *98*, 22,931-22,936, 1993.

Hanson, D. R., and A. R. Ravishankara, Reactive uptake of $ClONO_2$ onto sulfuric acid due to reaction with HCl and H_2O, *J. Phys. Chem.*, *98*, 5728-5735, 1994.

Hanson, D. R., A. R. Ravishankara, and S. Solomon, Heterogeneous reactions in sulfuric acid aerosols: A framework for model calculations, *J. Geophys. Res.*, *99*, 3615-3629, 1994.

Hübler, G., D. W. Fahey, K. K. Kelly, D. D. Montzka, M. A. Carroll, A. F. Tuck, L. E. Heidt, W. H. Pollock, G. L. Gregory, and J. F. Vedder, Redistribution of reactive odd nitrogen in the lower Arctic stratosphere, *Geophys. Res. Lett.*, *17*, 453-456, 1990.

Iraci, L. T., A. M. Middlebrook, and M. A. Tolbert, Laboratory studies of the formation of polar stratospheric clouds: Nitric acid condensation on thin sulfuric acid films, *J. Geophys. Res.*, *100*, 20,969-20,977, 1995.

Jonsson, H. H., et al., Performance of a focused cavity aerosol spectrometer for measurements in the stratosphere of particle size in the 0.06-2.0-μm-diameter range, *J. Atmos. Oceanic Technol.*, *12*, 115-129, 1995.

Kawa, S. R., D. W. Fahey, K. K. Kelly, J. E. Dye, D. Baumgardner, B. W Gandrud, M. Loewenstein, G. V. Ferry, and K. R. Chan, The Arctic polar stratospheric cloud aerosol: Measurements of reactive nitrogen, total water, and particles, *J. Geophys. Res.*, *97*, 7925-7938, 1992.

Kawa, S. R., et al., Activation of chlorine in sulfate aerosol as inferred from aircraft observations, *J. Geophys. Res.*, *102*, 3921-3933, 1997.

Keim, E. R., et al., Measurements of the NO_y-N_2O correlation in the lower stratosphere: Latitudinal and seasonal changes and model comparisons, *J. Geophys. Res.*, this issue.

Kelly, K. K., et al., Dehydration in the lower Antarctic stratosphere during late winter and early spring, 1987, *J. Geophys. Res.*, *94*, 11,317-11,357, 1989.

Koop, T., and K. S. Carslaw, Melting of H_2SO_4•$4H_2O$ particles upon cooling: Implications for polar stratospheric clouds, *Science*, *272*, 1638-1641, 1996.

Koop, T., U. M. Biermann, W. Raber, B. Luo, P. J. Crutzen, and T. Peter, Do stratospheric aerosol droplets freeze above the ice frost point?, *Geophys. Res. Lett.*, *22*, 917-920, 1995.

Kusik, C. L., and H. P. Meissner, Electrolyte activity coefficients in inorganic processing, *AIChE Symp. Ser.*, *74*, 14-20, 1978.

McElroy, M. B., R. J. Salawitch, and S. C. Wofsy, Antarctic O_3: Chemical mechanisms for the spring decrease, *Geophys. Res. Lett.*, *13*, 1296-1299, 1986.

Meilinger, S. K., T. Koop, B. P. Luo, T. Huthwelker, K. S. Carslaw, U. Krieger, P. J. Crutzen, and T. Peter, Size-dependent stratospheric droplet composition in lee wave temperature fluctuations and their potential role in PSC freezing, *Geophys. Res. Lett.*, *22*, 3031-3034, 1995.

Middlebrook, A. M., B. S. Berland, S. M. George, M. A. Tolbert, and O. B. Toon, Real refractive indices of infrared-characterized nitric-acid/ice films: Implications for optical measurements of polar stratospheric clouds, *J. Geophys. Res.*, *99*, 25,655-25,666, 1994.

Molina, M. J., R. Zhang, P. J. Wooldridge, J. R. McMahon, J. E. Kim, H. Y. Chang, and K. D. Beyer, Physical chemistry of the $H_2SO_4/HNO_3/H_2O$ system: Implications for polar stratospheric clouds, *Science*, *261*, 1418-1423, 1993.

Murphy, D. M., and B. L. Gary, Mesoscale temperature fluctuations and polar stratospheric clouds, *J. Atmos. Sci.*, *52*, 1753-1760, 1995.

Pawson, S., B. Naujokat, and K. Labitzke, On the polar stratospheric cloud formation potential of the northern stratosphere, *J. Geophys. Res.*, *100*, 23,215-23,225, 1995.

Peter, T., C. Brühl, and P. J. Crutzen, Increase in the PSC-formation probability caused by high-flying aircraft, *Geophys. Res. Lett.*, *18*, 1465-1468, 1991.

Pitari, G., V. Ritzi, L. Ricciardulli, and G. Visconti, High-speed civil transport impact: Role of sulfate, nitric acid trihydrate, and ice aerosols studied with a two-dimensional model, including aerosol physics, *J. Geophys. Res.*, *98*, 23,141-23,164, 1993.

Poole, L. R., and M. P. McCormick, Airborne lidar observations of Arctic polar stratospheric clouds, *Geophys. Res. Lett.*, *15*, 21-23, 1988.

Pruppacher, H. R., and J. D. Klett, *Microphysics of Clouds and Precipitation*, D. Reidel, Norwell, Mass, 1978.

Pueschel, R. F., et al., Condensed nitrate, sulfate, and chloride in Antarctic stratospheric aerosols, *J. Geophys. Res.*, *94*, 11,271-11,284, 1989.

Ravishankara, A. R., and D. R. Hanson, Differences in the reactivity of Type I PSCs depending on their phase, *J. Geophys. Res.*, *101*, 3885-3890, 1996.

Rosen, J. M., N. T. Kjome, and S. J. Oltmans, Simultaneous ozone and polar stratospheric cloud observations at South Pole station during winter and spring 1991, *J. Geophys. Res.*, *98*, 12,741- 12,751, 1993.

Rosenlof, K. H., A. F. Tuck, K. K. Kelly, J. M. Russell III, and M. P. McCormick, Hemispheric asymmetries in water vapor and inferences about transport in the lower stratosphere, *J. Geophys. Res.*, this issue

Smith, R. H., Formation of nitric acid hydrates: A chemical equilibrium approach, *Geophys. Res. Lett.*, *17*, 1291-1294, 1990.

Smithsonian Institution, *Smithsonian Meteorological Tables*, 6th rev. ed., prepared by R. J. List, *Smithson. Inst. Publ. 4014*, 350 pp., Washington, D.C., 1958.

Solomon, S., The mystery of the Antarctic ozone "hole," *Rev. Geophys.*, *26*, 131-148, 1988.

Solomon, S., Progress towards a quantitative understanding of Antarctic ozone depletion, *Nature*, *347*, 347-354, 1990.

Steele, H. M., and P. Hamill, Effects of temperature and humidity on the growth and optical properties of sulfuric acid-water droplets in the stratosphere, *J. Aerosol Sci.*, *12*, 517-528, 1981.

Stefanutti, L., M. Morandi, M. Del Guasta, S. Godin, and C. David, Unusual PSCs observed by LIDAR in Antarctica, *Geophys. Res. Lett.*, *22*, 2377-2380, 1995.

Stolarski, R. S., *et al., 1995 Scientific Assessment of the Atmospheric Effects of Stratospheric Aircraft, NASA Ref. Publ. 1381*, Washington, D.C., 1995.

Tabazadeh, A., and O. B. Toon, Freezing behavior of stratospheric sulfate aerosols inferred from trajectory studies, *Geophys. Res. Lett.*, *22*, 1725-1728, 1995.

Tabazadeh, A., and O. B. Toon, The presence of metastable HNO_3/H_2O solid phases in the stratosphere inferred from ER-2 data, *J. Geophys. Res.*, *101*, 9071-9078, 1996.

Tabazadeh, A., R. P. Turco, K. Drdla, and M. Z. Jacobson, A study of Type I polar stratospheric cloud formation, *Geophys. Res. Lett.*, *21*, 1619-1622, 1994a.

Tabazadeh, A., R. P. Turco, and M. Z. Jacobson, A model for studying the composition and chemical effects of stratospheric aerosols, *J. Geophys. Res.*, *99*, 12897-12914, 1994b.

Taesler, I., R. G. Delaplane, and I. Olovsson, Hydrogen bond studies, XCIV, Diaquaoxonium ion in nitric acid trihydrate, *Acta Crystallogt., Ser. B31*, 1489-1492, 1975.

Tie, X., X. Lin, and G. P. Brasseur, Two-dimensional coupled dynamical/chemical/microphysical simulation of global distribution of El Chichón volcanic aerosols, *J. Geophys. Res.*, *99*, 16,779-16,792, 1994.

Tolbert, M. A., M. J. Rossi, R. Malhotra, and D. M. Golden, Reaction of chlorine nitrate with hydrogen chloride and water at Antarctic stratospheric temperatures, *Science*, *238*, 1258-1260, 1987.

Toon, O. B., and M. A. Tolbert, Spectroscopic evidence against nitric acid trihydrate in polar stratospheric clouds, *Nature*, *375*, 218-221, 1995.

Toon, O. B., P. Hamill, R. P. Turco, and J. Pinto, Condensation of HNO_3 and HCl in the winter polar stratospheres, *Geophys. Res. Lett.*, *13*, 1284-1287, 1986.

Toon, O. B., E. V. Browell, S. Kinne, and J. Jordan, An analysis of lidar observations of polar stratospheric clouds, *Geophys. Res. Lett.*, *17*, 393-396, 1990.

Tuck, A. F., K. K. Kelly, C. R. Webster, M. Loewenstein, R. M. Stimpfle, M. H. Proffitt, and R. K, Chan, Airborne chemistry and dynamics at the edge of the 1994 Antarctic vortex, *J. Chem., Soc. Faraday Trans.*, *91*, 3063-3071, 1995.

Webster, C. R., R. D. May, and C. A. Trimble, Aircraft (ER-2) Laser Infrared Absorption Spectrometer (ALIAS) for *in-situ* stratospheric measurements of HCl, N_2O, CH_4, NO_2, and HNO_3, *Appl. Opt.*, *33*, 454-472, 1994.

Weisenstein, D. K., M. K. W. Ko, N. D. Sze, and J. M. Rodriguez, Potential impact of SO_2 emissions from stratospheric aircraft on ozone, *Geophys. Res. Lett.*, *23*, 161-164, 1996.

World Meteorological Organization (WMO), *Scientific Assessment of Ozone Depletion: 1994, WMO Rep. 37*, Global Ozone Res. and Monit. Proj., Geneva, 1995.

Worsnop, D. R., L. E. Fox, M. S. Zahniser, and S. C. Wofsy, Vapor pressures of solid hydrates of nitric acid: Implications for polar stratospheric clouds, *Science*, *259*, 71-74, 1993.

Zhang, R., P. J. Wooldridge, J. P. D. Abbatt, and M. J. Molina, Vapor pressure measurements for the $H_2SO_4/HNO_3/H_2O$ and

$H_2SO_4/HCl/H_2O$ systems: Incorporation of stratospheric acids into background sulfate aerosols, *J. Phys. Chem.*, *97*, 8541-8548, 1993.

Zhang, R., M. T. Leu, and L. F. Keyser, Hydrolysis of N_2O_5 and $ClONO_2$ on the $H_2SO_4/HNO_3/H_2O$ ternary solutions under stratospheric conditions, *Geophys. Res. Lett.*, *22*, 1493-1496, 1995.

D. Baumgardner, J. E. Dye, B. Gandrud, National Center for Atmospheric Research, Boulder, CO 80307

K. R. Chan, M. Loewenstein, J. R. Podolske, A. Tabazadeh, NASA Ames Research Center, Moffett Field, CA 94035

L. A. Del Negro (corresponding author), R/E/AL6, NOAA Aeronomy Laboratory, 325 Broarway, Boulder, CO 80303; Cooperative Institute for Research in Environmental Science (CIRES), University of Colorado, Boulder 80309; and Department of Chemistry and Biochemistry, University of Colorado, Boulder, CO 80309. (e-mail: delnegro@al.noaa.gov)

S. G. Donnelly, R. S. Gao, R. C. Wamsley, NOAA Aeronomy Laboratory and CIRES.

D. W. Fahey, E. R. Keim, K. K. Kelly, NOAA Aeronomy Labora tory.

H. H. Jonsson, J. C. Wilson, Department of Engineering, University of Denver, Denver, CO 80208

R. D. May, C. R. Webster, Jet Propulsion Laboratory, California Institute of Technology, Pasadena, CA 91109

M. A. Tolbert, CIRES and Department of Chemistry and Biochemistry, University of Colorado.

E. L. Woodbridge, Scripps Institution of Oceanography, University of California at San Diego, La Jolla, CA 92093.

D. R. Worsnop, Aerodyne Research, Inc., Billerica, MA 02139

(Received July 1, 1996; revised February 28, 1997;
accepted March 3, 1997)